

SHEAR STRENGTH OF END REGIONS OF PRESTRESSED
SELF-CONSOLIDATING CONCRETE BEAMS

Except where reference is made to the work of others, the work described in this thesis is my own or was done in collaboration with my advisory committee. This thesis does not include proprietary or classified information.

Mustafa İspir Gürbüz

Certificate of Approval:

Anton K. Schindler
Gottlieb Associate Professor
Civil Engineering

Robert W. Barnes, Chair
James J. Mallett Associate Professor
Civil Engineering

Mary L. Hughes
Assistant Professor
Civil Engineering

Joe F. Pittman
Interim Dean
Graduate School

SHEAR STRENGTH OF END REGIONS OF PRESTRESSED
SELF-CONSOLIDATING CONCRETE BEAMS

Mustafa İspir Gürbüz

A Thesis

Submitted to

the Graduate Faculty of

Auburn University

in Partial Fulfillment of the

Requirements for the

Degree of

Master of Science

Auburn, Alabama
May 10, 2008

SHEAR STRENGTH OF END REGIONS OF PRESTRESSED
SELF-CONSOLIDATING CONCRETE BEAMS

Mustafa İspir Gürbüz

Permission is granted to Auburn University to make copies of this thesis at its discretion, upon request of individuals or institutions and at their expense. The author reserves all publication rights.

Signature of Author

Date of Graduation

VITA

Mustafa İspir Gürbüz, son of Fikret and Nuran Gürbüz, was born July 8, 1984, in Ankara, Turkey. He graduated from TED Ankara College Private High School in 2001. He attended Middle East Technical University in Ankara, Turkey and graduated as a high honor student in June 2005 with a Bachelor of Science degree in Civil Engineering with Structural Mechanics as undergraduate specialization. He entered Graduate School at Auburn University in January 2006.

THESIS ABSTRACT

SHEAR STRENGTH OF END REGIONS OF PRESTRESSED
SELF-CONSOLIDATING CONCRETE BEAMS

Mustafa İspir Gürbüz

Master of Science, May 10, 2008
(B.S., Middle East Technical University, Ankara, Turkey, 2005)

108 Typed Pages

Directed by Robert W. Barnes

Understanding of the shear and bond performance of self-consolidating concrete (SCC) is vital to fully implement SCC usage in structures. State highway structures are a potential application for prestressed SCC systems once more knowledge is gained regarding this performance.

In order to investigate the shear and bond performance of end regions of prestressed SCC beams, several conventional and SCC prestressed T-beams were tested in flexure with unequal shear spans. Displacement and strand end slip were measured as the specimens were loaded to failure. These results are provided together with behavioral descriptions. Results were analyzed using flexural beam theory and AASHTO LRFD design provisions.

It was concluded that AASHTO LRFD shear specifications provide overly conservative provisions for high strength (SCC) beams not fully utilizing superior bond characteristics of SCC systems.

ACKNOWLEDGEMENTS

Funding of this research was provided by the Alabama Department of Transportation.

I would like to thank Dr. Robert W. Barnes for his continuous support, encouragement and understanding throughout my study in Auburn. I would like to thank my committee members Dr. Mary L. Hughes and Dr. Anton K. Schindler for their invaluable advice and help. I would also like to thank Billy Wilson for all his help during the experiments.

I would like to thank my Middle East Technical University professors Dr. Cem Topkaya for helping me get to Auburn as well as Dr. Uğur Ersoy, to whom I owe my love for my profession.

Style manual used

Chicago Manual of Style

Computer software used

Microsoft Word, Microsoft Excel

TABLE OF CONTENTS

LIST OF FIGURES	xiii
LIST OF TABLES	xvi
CHAPTER 1. INTRODUCTION	1
1.1. Background	1
1.2. Research Objectives	2
1.3. Research Scope	2
1.4. Organization of Thesis	3
1.5. Notation	4
CHAPTER 2. BACKGROUND ON THE DESIGN OF REINFORCED CONCRETE BRIDGE SYSTEMS TO RESIST SHEAR	5
2.1. Shear Behavior	5
2.2. Principal Stress Analyses	6
2.3. Mohr's Circle	6
2.4. Diagonal Cracking	8
2.4.1. Flexure-shear cracking	8
2.4.2. Web-shear cracking	9
2.5. Behavior After Diagonal Cracking	9
2.6. Failure Modes	9

2.7. Compression Field Theory.....	11
2.8. Modified Compression Field Theory.....	12
2.9. AASHTO Shear Provisions	14
2.9.1. Sectional design method	14
2.9.2. General procedure.....	14
2.9.3. Simplified procedure.....	16
2.9.4. Minimum transverse reinforcement requirement.....	16
2.9.5. Maximum aggregate size	17
2.9.6. Longitudinal reinforcement demand.....	18
2.9.7. Critical section for shear	19
2.9.8. Strut-and-Tie Modeling	19
2.10. Simplified Modified Compression Field Theory.....	20
2.11. High-Strength Concrete	20
CHAPTER 3. SPECIMEN PROPERTIES AND TESTING.....	21
3.1. Introduction.....	21
3.2. Specimen Identification	22
3.3. Material Properties.....	24
3.3.1. Prestressing steel.....	24
3.3.2. Mild reinforcing steel.....	24
3.3.3. Concrete	25
3.4. Prestressing Parameters	28
3.5. Test Setup and Instrumentation	28
3.6. Instrumentation	32

3.6.1. Measurement of applied load.....	32
3.6.2. Measurement of displacements.....	33
3.6.3. Measurement of strand slip.....	34
3.6.4. Measurement of strains at extreme compression fibers.....	34
3.6.5. Data acquisition	35
CHAPTER 4. TEST RESULTS	36
4.1. Introduction.....	36
4.2. Specimen STD-M-E.....	36
4.3. Specimen STD-M-W	42
4.4. Specimen SCC-MS-E	46
4.5. Specimen SCC-HS-W.....	50
4.6. Specimen SCC-HS-E.....	53
4.7. Summary of Test Results.....	57
CHAPTER 5. ANALYSIS AND DISCUSSION	59
5.1. Flexural Analysis	59
5.2. AASHTO LRFD Shear Analyses	66
5.2.1. Shear cracking.....	66
5.2.2. Shear capacity	69
5.2.3. Post-cracking tension demand	71
5.3. Transverse Reinforcement	75
5.3.1. Effect of transverse reinforcement on post-cracking tension demand.....	75
5.3.2. Transverse reinforcement spacing	78
CHAPTER 6. CONCLUSION AND RECOMMENDATIONS	83

6.1. Summary	83
6.2. Conclusions.....	83
6.3. Recommendations.....	85
REFERENCES	86
APPENDIX A. NOTATION	89

LIST OF FIGURES

Figure 2-1. Width-averaged shear stress distributions on rectangular and T sections.....	5
Figure 2-2. Mohr's Circles for nonprestressed and prestressed beam elements.....	7
Figure 2-3. Flexure-shear and web-shear cracks (Naaman 2004)	8
Figure 2-4. Major shear failure modes (Naaman 2004).....	10
Figure 2-5. Stress-strain relationship for cracked concrete in compression	12
Figure 2-6. 3-D Representation of compressive stress-strain relationship	13
Figure 2-7. Average stress strain relationship for concrete in tension.....	13
Figure 3-1. Specimen cross section detail (Levy 2007).....	22
Figure 3-2. Specimen identification system of Levy (2007)	23
Figure 3-3. Specimen identification system used in this study.....	24
Figure 3-4. Test setup diagram	29
Figure 3-5 Test setup	29
Figure 3-6. Neoprene pads, steel supports and concrete blocks	31
Figure 3-7. Hydraulic actuator and force transducer	32
Figure 3-8. Potentiometers.....	33
Figure 3-9. Strand slip measurement	34
Figure 3-10. Data acquisition system.....	35
Figure 4-1. Applied load and strand slips vs. load point displacement - STD-M-E.....	37
Figure 4-2. Initial crack at 32 kips applied load – STD-M-E	38

Figure 4-3. Final state of crack at the end of test– STD-M-E.....	39
Figure 4-4. Shear tension failure showing loss of bond – STD-M-E	39
Figure 4-5. Load point displacement and strand slip versus time – STD-M-E	40
Figure 4-6. Applied load and strand slip versus time – STD-M-E	41
Figure 4-7. Applied load and strand slips versus load point displacement - STD-M-W..	42
Figure 4-8. STD-M-W: Initial crack at 27.2 kips applied load - STD-M-W	43
Figure 4-9. STD-M-W: Final state of crack at the end of test - STD-M-W	44
Figure 4-10. Load point displacement and strand slip versus time - STD-M-W	45
Figure 4-11. Applied load and strand slip versus time - STD-M-W	45
Figure 4-12. Applied load and strand slips versus load point displacement - SCC-MS-E	46
Figure 4-13. Flexural cracks under load point at 51kips applied load - SCC-MS-E	47
Figure 4-14. Flexural cracks under load point at 56 kips applied load - SCC-MS-E	48
Figure 4-15. Final condition of flexural cracks at the end of test - SCC-MS-E	48
Figure 4-16. Final condition at the end of test - SCC-MS-E	49
Figure 4-17. Applied load and strand slips versus load point displacement - SCC-HS-W	50
Figure 4-18. Flexural cracks under load point at 48 kips applied load - SCC-HS-W	51
Figure 4-19. Final condition of flexural cracks at the end of test - SCC-HS-W.....	52
Figure 4-20. Final condition at the end of test - SCC-HS-W	52
Figure 4-21. Applied load and strand slips versus load point displacement - SCC-HS-E	53
Figure 4-22. Shear crack at 66 kips cracking load - SCC-HS-E.....	54
Figure 4-23. Final state of the shear crack at the end of test - SCC-HS-E	55
Figure 4-24. Load point displacement and strand slip versus time - SCC-HS-E	56

Figure 4-25. Applied load and strand slip versus time - SCC-HS-E	56
Figure 5-1. Layers for sectional analysis	60
Figure 5-2. Concrete fibers affected by tension stiffening	61
Figure 5-3. Flexural analysis result for STD-M-E.....	62
Figure 5-4. Flexural analysis result for STD-M-W	63
Figure 5-5. Flexural analysis result for SCC-MS-E.....	63
Figure 5-6. Flexural analysis result for SCC-HS-W	64
Figure 5-7. Flexural analysis result for SCC-HS-E	64
Figure 5-8. Experimental versus valculated V_c values.....	68
Figure 5-9. V_c as function of ϵ_x for $s_{xe} \leq 15$ in.....	69
Figure 5-10. Applied load at strand tension capacity for specimen STD-M-E	73
Figure 5-11. Applied load at strand tension capacity for specimen STD-M-W	74
Figure 5-12. Applied load at strand tension capacity for specimen SCC-HS-E.....	74
Figure 5-13. Applied load at strand tension capacity for specimen STD-M-E with and without transverse reinforcement.....	76
Figure 5-14. Applied load at strand tension capacity for specimen STD-M-W with and without transverse reinforcement.....	77
Figure 5-15. Applied load at strand tension capacity for specimen SCC-HS-E with and without transverse reinforcement.....	78
Figure 5-16. Diagonal crack location of specimen STD-M-E.....	80
Figure 5-17. Diagonal crack location of specimen SCC-HS-E	80
Figure 5-18. Diagonal crack location of specimen SCC-M-W.....	81
Figure 5-19. s_{max} (maximum stirrup spacing) versus of d_v (effective shear depth).....	82

LIST OF TABLES

Table 3-1. Mixture properties	26
Table 3-2. Fresh properties	27
Table 3-3. Hardened properties.....	27
Table 3-4. Previous testing results	28
Table 3-5. Test configuration dimensions and strand release conditions	30
Table 4-1. Specimen cracking and ultimate loads and failure modes.....	57
Table 4-2. Crack positions of specimens	58
Table 5-1. Loads corresponding to flexural cracking and ultimate strength	65
Table 5-2. Cracking moments corresponding to crack locations.....	65
Table 5-3. Shear capacity calculations based on applied maximum shear	70
Table 5-4. Shear capacity calculations based on $V_n = V_u$	71
Table 5-5. Tension demands compared to tension capacities.....	72
Table 5-6. Cracking loads and reserve strengths of specimens	79

Chapter 1. Introduction

1.1. Background

Prestressed concrete is used as an efficient structural system for various applications worldwide. Prestressed, especially precast, concrete elements are preferred over conventionally reinforced concrete elements in many applications due to the efficiency and versatility they provide in construction, as well as their inherent durability. Use of high strength concrete has accelerated the widespread use of prestressed concrete elements. High-strength, self-consolidating concrete (SCC), however, has not yet been fully employed in prestressed concrete bridge structures because of lack of structural performance data related to its use.

SCC, first developed in Japan in 1980's, can be placed without time-consuming and costly vibration procedures, thereby making it economically beneficial. Although SCC is favored by the industry due to its efficiency in placing and finishing, some official specifications do not yet permit the use of SCC in prestressed concrete applications. Approval of the use of SCC in prestressed systems by transportation agencies awaits the results of further research. For example, shear and bond performance of prestressed SCC is a source of debate among researchers, transportation agencies and the industry. Shear and bond performance of SCC is an important issue because of the increased fine aggregate content that aids in creating the flowability of SCC.

1.2. Research Objectives

The Alabama Department of Transportation (ALDOT) has sponsored an investigation by the Auburn University Highway Research Center into the use of SCC in prestressed concrete bridge girders. The primary objectives of the investigation are to:

- Develop SCC mixtures for use in prestressed concrete bridge structures,
- Evaluate the behavior of SCC mixtures in prestressed concrete girders, including fresh properties, early-age behavior, and long-term behavior, and
- Develop implementation guidelines and recommendations for industry use.

The study presented in this thesis is a portion of the aforementioned project. The primary objective of this study was to evaluate the shear and bond behavior of prestressed reinforcement in beams constructed with SCC and to evaluate the long-term performance of SCC when used in prestressed concrete girders.

1.3. Research Scope

This study consisted of an experimental investigation into the shear behavior of prestressed concrete beams. Five specimens, which were portions of beams previously tested by Levy (2007), were tested: two were made of conventional moderate-strength concrete, one was made with moderate-strength SCC and the remaining two were made of high-strength SCC. All of these mixtures were designed for implementation in pretensioned concrete bridge girders. Each of the five specimens was tested to failure with single-point loading positioned to create unequal shear spans. The behavior of the test specimens was compared with flexural analysis results and the provisions of American Association of State Highway and Transportation Officials Load and

Resistance Factor Design (AASHTO LRFD) Bridge Design Specifications (2007) for shear.

The mixing, fabrication, measurements, and testing of the beams were performed in the Structural Engineering Laboratory of the Auburn University Department of Civil Engineering.

1.4. Organization of Thesis

Chapter 2 provides a literature review including basic principles of shear behavior in structural concrete. Several theories developed to understand shear behavior of reinforced and prestressed concrete members are presented. AASHTO LRFD Specifications (AASHTO LRFD 2007) on shear design and analysis are described, including assumptions and rationalizations on which several approaches are founded.

Chapter 3 provides a description of the design and fabrication of the prestressed specimens. The results of fresh and hardened property testing of the concrete mixtures as well as other experimental results obtained by Levy (2007) are presented in this chapter. The test setup and instrumentation are also presented in this chapter.

Chapter 4 provides the results of the conducted experiments that were conducted. The behavior of each specimen during testing is described in detail.

Chapter 5 provides flexural and shear analysis results and comparisons with relevant test data. Several outcomes of such comparisons and other observed testing behavior are also discussed in this chapter.

Chapter 6 offers conclusions based on the work documented in this thesis. Recommendations for further research are also provided within this chapter.

1.5. Notation

The notation used in this document mainly follows the notation outlined in the *AASHTO LRFD Bridge Design Specifications* (2007). A list of the notation used throughout is presented in Appendix A.

Chapter 2. Background on the Design of Reinforced Concrete Bridge Systems to Resist Shear

2.1. Shear Behavior

External forces acting on structures cause shear stresses in addition to axial and flexural effects. Unlike normal stresses caused by axial forces, shear stresses are not distributed linearly over the depth of flexural members. However, they are fairly constant across the cross-sectional dimension perpendicular to the applied load (i.e. width); therefore, the width-averaged value is often used for simplicity. Width-averaged shear stress distributions across the depth of typical homogeneous, isotropic, and linearly elastic rectangular and T-shaped cross sections can be seen in Figure 2-1.

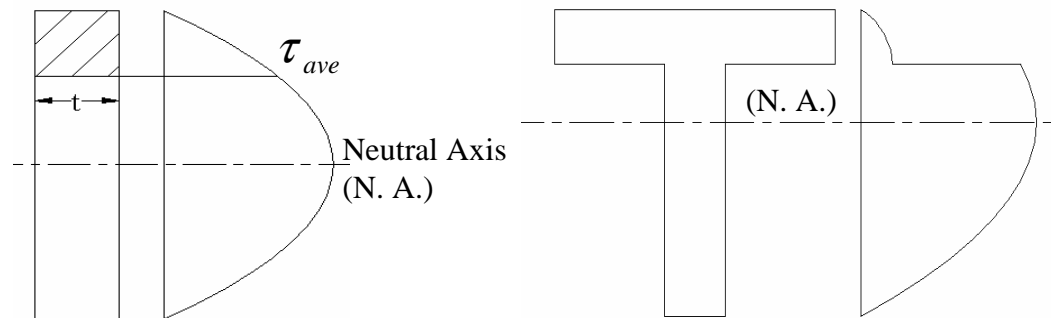


Figure 2-1. Width-averaged shear stress distributions on rectangular and T sections

Theoretical shear stress distributions assume second-degree polynomial curve shapes and reach maximum values at the centroid. Average shear stress (τ_{ave}) on a horizontal section of a beam can be calculated using:

$$\tau_{ave} = \frac{VQ}{It}$$

where V is the shear force, Q is the first moment of the area of the shaded section with respect to the neutral axis, I is the moment of inertia of the cross section about the neutral axis, and t is the width of the section at the point of interest (Beer and Johnson 1992).

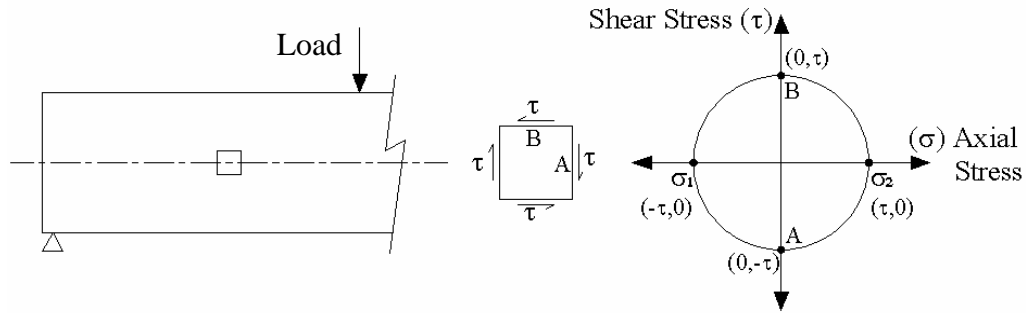
2.2. Principal Stress Analyses

The shear strength of concrete is much higher than its tensile strength. Therefore, shear stresses are not direct causes of cracking in concrete. Moreover, shear stresses are seldom observed by themselves; most of the time they are accompanied by axial stresses.

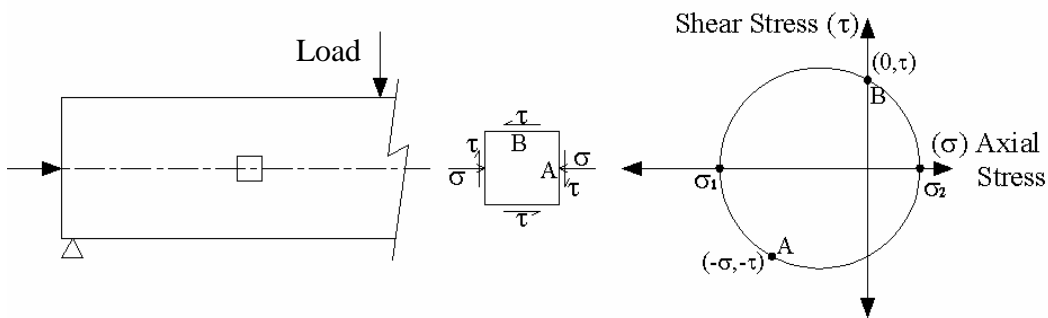
Principal stress analysis is required to understand the resulting effects of axial and/or shear stresses.

2.3. Mohr's Circle

In order to obtain principal stresses, σ_1 (minimum) and σ_2 (maximum), at a point in a beam, Mohr's Circle analysis can be used. Mohr's Circles of typical concrete elements from nonprestressed and prestressed beams are shown in Figure 2-2. Tensile stresses are shown as positive.



Nonprestressed beam element at centroid



Prestressed beam element at centroid

Figure 2-2. Mohr's Circles for nonprestressed and prestressed beam elements

It can be seen that axial compressive stresses caused by prestressing forces significantly reduce principal tensile stresses that result from shear stress. The largest tensile principal stresses, compared to the tensile strength or modulus of rupture values of concrete, can be calculated at specific loadings to predict diagonal cracking loads. Diagonal tensions are of concern because they lead to cracking of concrete due to its relative low tensile strength (Naaman 2004). Element failures that are called shear failures are mostly diagonal tension failures or sometimes diagonal compression failures, since true shear failure at the material level is rarely observed (Ferguson et al. 1988).

2.4. Diagonal Cracking

When principal tensile stresses existing at various angles with the horizontal reach critical values they cause cracking in the concrete. These inclined cracks are called diagonal cracks and several researchers classify diagonal cracking into two main types: flexure-shear cracking and web-shear cracking (Sozen and Hawkins 1962; MacGregor et al. 1965; Lorentsen 1965). These two main shear cracks are shown in Figure 2-3.

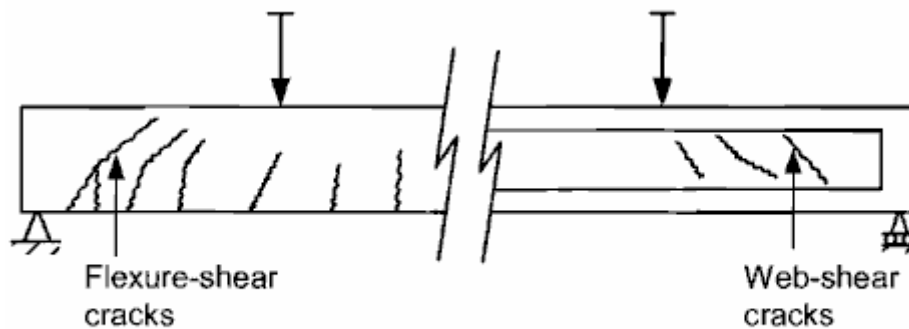


Figure 2-3. Flexure-shear and web-shear cracks (Naaman 2004)

Diagonal cracks are not fully restrained by longitudinal reinforcement and usually transverse reinforcement is required to avoid brittle failures (Nawy 2006). Because crack locations are discrete and the material is no longer isotropic, diagonal cracks make average constitutive (stress-strain) relationships complex (Collins 1978).

2.4.1. Flexure-shear cracking

Flexure-shear cracks are observed to start at, or in the vicinity of, flexural cracks and they quickly propagate in an inclined path (Bresler and MacGregor 1967). The propagation path is along the (diagonal) plane of principal tension (Naaman 2004). After flexural cracking, significant stress redistributions occur; this makes it difficult to accurately

predict (1) the load that causes a flexure crack to transform into a flexure-shear crack and (2) the shear that can be resisted by the concrete after the formation of a flexure-shear crack in a reinforced beam (Bresler and MacGregor 1967; Collins and Mitchell 1997).

2.4.2. Web-shear cracking

Web-shear cracking is observed before flexural cracking, especially in beams with narrow webs. In regions where shear force is high relative to bending moment, a diagonal tension crack often occurs before a flexural crack because diagonally aligned principal tensile stresses near the centroid are relatively higher than flexural stresses near the tension face (Naaman 2004). Usually prestressing forces delay the formation of flexural cracks, which can result in web-shear cracks appearing first in high-shear regions of prestressed beams (MacGregor and Hanson 1969). Since web-shear cracking happens before any flexural cracking, principal stresses leading to cracking can be calculated more accurately (Bresler and MacGregor 1967).

2.5. Behavior After Diagonal Cracking

After diagonal cracks form, concrete contribution to shear stress transmission is greatly reduced. Adequate transverse and longitudinal reinforcement is required to balance these stresses (Collins and Mitchell 1997). Although diagonal cracking is not a failure mode of reinforced members by itself, it is a major contributor to the final failure of members.

2.6. Failure Modes

Flexure-shear cracking or web-shear cracking may lead to several shear failure modes. Shear span to depth ratio (a/d) is used as a classification parameter for failure modes.

Major types that can be observed in slender ($a/d > 2.5$) to short ($1 < a/d < 2.5$), rectangular and I-beams are: diagonal tension failure, web crushing failure, shear tension failure and shear compression failure as shown in Figure 2-4 (Bresler and MacGregor 1967; ASCE-ACI 1973).

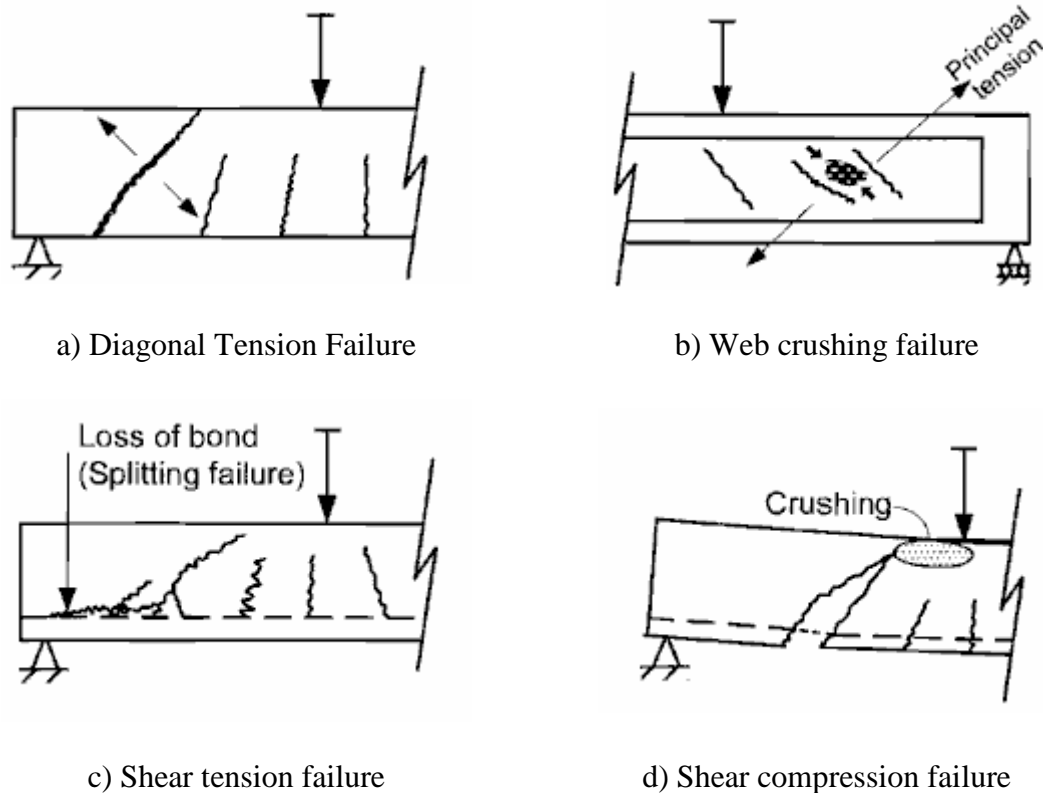


Figure 2-4. Major shear failure modes (Naaman 2004)

Diagonal tension failure is usually observed in moderately slender beams. In this case, a web-shear or flexural-shear crack propagates throughout the depth of the beam causing a failure. Web crushing failure is observed typically in I-beams with narrow webs. Web crushing is caused after web-shear cracking by excessive compressive stresses on the diagonal compression elements. Shear tension failure is observed in short beams when a secondary crack forms branching off a shear crack at the level of longitudinal reinforcement and propagates towards the beam end. This secondary crack

causes a loss of bond resulting in an anchorage failure of the longitudinal reinforcement. (Bresler and MacGregor 1967; ASCE-ACI 1973). In addition, the diagonal nature of shear cracking can result in a tension demand on the flexural reinforcement that is larger than what would be computed by only considering bending moment at a section (Ferguson et al. 1988). When an anchorage failure does not occur, the concrete at the compression (upper) end of the crack may fail in crushing. This type of failure is called shear compression failure (Naaman 2004).

2.7. Compression Field Theory

Compression Field Theory was presented by Michael P. Collins in 1978. It is based on the assumptions that concrete carries no tension after it is cracked and it carries compression in forms similar to truss models. The diagonal compression field in concrete transmits the shear stresses (Collins 1978).

In this method of analysis, an implicit relationship is used between strain values and the angle of principal compression (θ). Having necessary equilibrium and compatibility equations determined, transverse, longitudinal and principal compression strains can be calculated using an assumed value of θ . Using these three strains, another estimate of the angle of principal compression is obtained, and an iterative trial-error solution is reached.

As an upper limit to the ultimate shear capacity (v_u) of a member after the transverse reinforcement yields, Compression Field Theory assumes that the longitudinal steel yields or the concrete compressive stress reaches its limiting value. This approach is expressed in the following equation (Collins 1978):

$$v_u \leq \sqrt{(\rho_t f_{ty}) \left(\rho_t f_{ly} + \rho_p f_{py} + \frac{N}{b_w jd} \right)} \text{ or } v_u \leq \sqrt{f_{du} \rho_t f_{ty} - (\rho_t f_{ty})^2}$$

where ρ stands for the reinforcement ratio, f_y for yield strength, N for axial force, b_w , web width, jd for effective depth of shear and f_{du} for the limiting value of the average principal compressive stress in concrete. Additional subscripts t , l and p stand for transverse and longitudinal mild reinforcement and prestressing steel, respectively (Collins 1978). It can also be added that the prestressing or mild reinforcing steel anchorage capacity also limits the ultimate capacity of the member when the section considered is within the transfer or development length regions.

2.8. Modified Compression Field Theory

Modified Compression Field Theory (MCFT) was presented by Frank J. Vecchio and Michael P. Collins in 1986 as a further development of the 1978 Compression Field Theory by Collins. After an experimental program involving tests of square reinforced concrete elements under well defined axial and shear loads, average stress versus average strain relationships, as shown in Figure 2-5 and Figure 2-6, were obtained for cracked, reinforced concrete under normal and shear stresses.

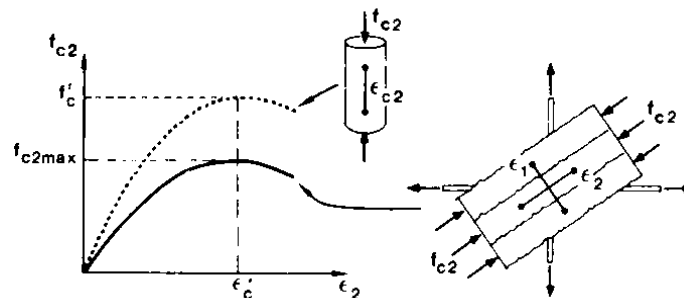


Figure 2-5. Stress-strain relationship for cracked concrete in compression

(Vecchio and Collins 1986)

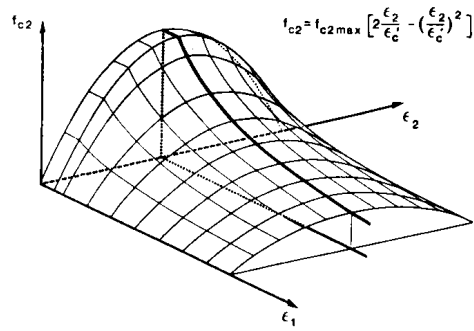


Figure 2-6. 3-D Representation of compressive stress-strain relationship
(Vecchio and Collins 1986)

In contrast to the original Compression Field Theory (Collins 1978), MCFT takes into account tensile stresses developed in the concrete between the cracks (tension stiffening). Tensile behavior of concrete is modeled as shown in Figure 2-7.

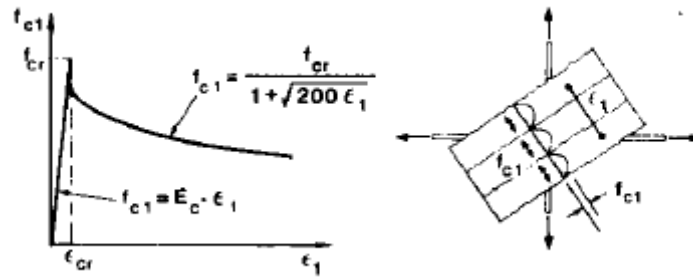


Figure 2-7. Average stress strain relationship for concrete in tension
(Vecchio and Collins 1986)

At crack points, steel may be assumed to have yielded, but between cracks steel may not have yielded because concrete carries some of the tensile stresses in that region (Vecchio and Collins 1986).

2.9. AASHTO Shear Provisions

AASHTO LRFD Bridge Design Specifications (AASHTO LRFD 2007) address shear and torsion in concrete structures in Section 5.8. Both Article 5.8.3 (Sectional Design Model) and Article 5.6.3 (Strut-and-Tie Model) can be applied to flexural regions where plane sections remain plane. For components in which the distance from the point of zero shear to the face of the support is less than twice the depth of the member, use of Article 5.6.3 is left to the engineer's discretion (AASHTO LRFD 2007).

2.9.1. Sectional design method

The Sectional Design Method is used to compare factored shear forces and factored shear resistances at sections along the span. The governing equations used to calculate resistance are Equations 5.8.3.3-1 to 5.8.3.3-4, which are used to calculate nominal shear resistance (V_n), nominal shear resistance provided by concrete (V_c) and nominal shear resistance provided by shear reinforcement (V_s). The component of effective prestressing force in the direction of the applied shear (V_p) is also used as a variable in the calculation of V_n .

For prestressed members, V_c can be calculated using either the General Procedure (Article 5.8.3.4.2) or the Simplified Procedure for Prestressed and Nonprestressed Sections (Article 5.8.3.4.3).

2.9.2. General procedure

The General Procedure (Article 5.8.3.4.2) is essentially an application of the Modified Compression Field Theory by Vecchio and Collins (1986), although this theory is not directly in the provisions. It is an iterative process that follows different paths depending

on the amount of transverse reinforcement supplied. Sections are divided into two categories having (1) at least equal to or (2) less than the minimum transverse reinforcement specified in Article 5.8.2.5. An iterative process, in both cases, is used to determine ϵ_x , the longitudinal strain in on the flexural tension side of the member. ϵ_x is then used to find β (factor relating ϵ_x to V_c , indicating the ability of diagonally cracked concrete to transmit tension and shear) and θ (angle of inclination of diagonal compressive stresses in degrees). For increased θ values, although V_c is decreased, V_s is increased due to the fact that principal tension orientation more closely aligns with the vertical orientation of transverse reinforcement.

For members having at least the minimum transverse reinforcement, shear-stress-to- f'_c ratio is used as the governing parameter for the tables used for the iterations of β and θ values. However, for members having less than the required minimum transverse reinforcement s_{xe} , a spacing parameter, is used. The spacing parameter is calculated as follows:

$$s_{xe} = s_x \frac{1.38}{a_g + 0.63} \leq 80 \text{ in.}$$

where:

s_x = the lesser of either d_v (effective shear depth) or maximum distance between layers of longitudinal crack control reinforcement (in.)

a_g = maximum aggregate size (in.)

2.9.3. Simplified procedure

For concrete beams having at least minimum transverse steel reinforcement and not subject to significant axial tension, a simplified procedure is suggested to calculate V_c . This method, in which V_c is taken as lesser of V_{ci} (nominal shear resistance provided by concrete when inclined cracking results from combined shear and moment) and V_{cw} (nominal shear resistance provided by concrete when inclined cracking results from excessive principal tensions in web), is similar to the ACI 318 (2005) approach and is based on recommendations by the NCHRP Report 549 (Hawkins et al. 2005).

2.9.4. Minimum transverse reinforcement requirement

In Article 5.8.2.5, AASHTO LRFD requires a minimum amount of transverse steel to control the diagonal cracks and increase ductility, as well as to provide post-cracking reserve strength. This minimum amount is required when the factored shear force is more than the half of the nominal shear resistance of the concrete added to the component of prestressing force in the direction of the shear force. Post-cracking reserve strength refers to the shear capacity of the member after diagonal cracking. The minimum transverse reinforcement requirement is defined by:

$$A_v \geq 0.0316 \sqrt{f'_c} \frac{b_v s}{f_y}$$

where:

A_v = area of a transverse reinforcement within distance s (in.²)

b_v = width of web (in.)

s = spacing of transverse reinforcement (in.)

f_y = yield strength of transverse reinforcement (ksi)

When the minimum transverse reinforcement requirement is substituted into the V_s and V_c equations as described in Article 5.8.3.3, the following equation is obtained:

$$V_s \geq \frac{V_c \cot \theta}{\beta}$$

This minimum transverse reinforcement requirement was analyzed by Ozcebe et al. (1999), Angelakos et al. (2001) and Rahal and Al-Shaleh (2004), and it was reported to be adequate. However, it was also reported that further testing was necessary to justify the validity of this requirement for high-strength concrete ($f_c' \geq 10$ ksi).

2.9.5. Maximum aggregate size

In the case of members with less than the minimum transverse reinforcement, concrete contribution to shear resistance is critical. Therefore, for a more accurate prediction of shear resistance, concrete-aggregate interlocking and other shear-friction factors need to be taken into greater account (Sherwood et al. 2007). When cracks widths increase, it has been seen that stresses that can be transmitted across cracks gradually decrease, indicating a certain transfer mechanism of interlocking grains (Moe 1962). It has been observed that close to sixty percent of the shear resistance is provided by the aggregate interlocking mechanism (Fenwick and Paulay 1968). In the application of the Modified Compression Field Theory, maximum aggregate size is used as a parameter in the determination of shear resistance due to aggregate interlock (Vecchio and Collins 1986).

When high-strength concrete ($f_c' \geq 10$ ksi) is used, the maximum aggregate size is recommended to be taken as zero (Bentz et al. 2006). This argument is considered valid because with high-strength concrete, aggregate interlocking does not play an important

role in transferring shear forces. This is due to the fact that aggregates are cut through in case of a diagonal crack in high-strength concrete.

2.9.6. Longitudinal reinforcement demand

Shear causes an axial tension demand in the longitudinal steel reinforcement—both in prestressing strands and in mild reinforcement. This demand, which is beyond the demand due to bending moment and axial force alone, has to be satisfied by the axial tension capacity of the longitudinal reinforcement. AASHTO LRFD (2007) specifications evaluate this capacity by assuming the mild steel reinforcement yields and the prestressing strands develop resistance in a linear or bi-linear fashion over the transfer and development lengths. AASHTO LRFD (2007) Article 5.8.3.5 requires the longitudinal reinforcement capacity to be larger than the longitudinal strength demand satisfying the following equations:

$$A_{ps}f_{ps} + A_s f_y \geq \frac{|M_u|}{d_v \phi_f} + 0.5 \frac{N_u}{\phi_c} + \left(\left| \frac{V_u}{\phi_v} - V_p \right| - 0.5V_s \right) \cot \theta$$

or

$$A_{ps}f_{ps} + A_s f_y \geq \left(\left| \frac{V_u}{\phi_v} - V_p \right| - 0.5V_s \right) \cot \theta \text{ (for the span between the face of the support}$$

and the critical section)

where:

A_{ps} = prestressing strand area (in.²)

f_{ps} = effective prestressing stress (ksi)

A_s = longitudinal mild reinforcement area (in.²)

f_y = yield strength of longitudinal mild reinforcement (ksi)

M_u = factored moment (kip-in.)

d_v = effective shear depth (in.)

N_u = factored axial force (kip)

V_u = factored shear force (kip)

V_p = component of effective prestressing force in the direction of the applied shear (kip)

V_s = nominal shear resistance provided by shear reinforcement (kip)

θ = angle of inclination of diagonal compressive stresses ($^\circ$)

ϕ_f , ϕ_v , ϕ_c = flexural, shear and compressive resistance factors, respectively

2.9.7. Critical section for shear

AASHTO LRFD (2007) Article 5.8.3.2 specifies the critical section for shear to be a distance of d_v (effective shear depth, as described in Article 5.8.2.9) from the internal face of the support. For the design of the portion of the span between the support face and the critical section, this section is used for all shear capacity calculations, as well as for tension demand calculations of longitudinal reinforcement. The basic assumption for this approach is that loads inside the span up to the critical section are directly transferred (without beam action) to the support (Naaman 1994).

2.9.8. Strut-and-Tie Modeling

In Article 5.8.1.1 of the AASHTO LRFD Bridge Design Specifications (2007), it is stated that if the point of zero shear is closer than two times the member depth to the face of the support it may be considered as a deep member. However, the AASHTO specifications are not clear about the requirement on the design or analysis method. It is stated in the commentary that the strut and tie model yields less conservative results for regions near

discontinuities. Therefore, it is understood that the strut and tie model can be used at the engineer's discretion in order to achieve more efficient designs.

2.10. Simplified Modified Compression Field Theory

In 2006, Bentz et al. introduced a simplified method based on the Modified Compression Field Theory. This new method, called Simplified Modified Compression Field Theory (SMCFT), is aimed at predicting shear strengths of members without the iterative procedures necessary with the MCFT. SMCFT presents closed-form equations, instead of the current AASHTO LRFD tables for the calculation of ϵ_s , θ and β values (Bentz et al. 2006).

SMCFT is also employed in the 2004 Canadian Standards Association (CSA) A23.3 shear provisions for reinforced concrete (Bentz and Collins 2006).

2.11. High-Strength Concrete

AASHTO LRFD specifications, in Article 5.4.2.1, imply that properties that might be related to concrete compressive strength are derived using compressive strengths of 10.0 ksi or less. It is advised to use concrete compressive strengths of 10.0 ksi or more only if relationships between such properties and concrete strengths are established by physical tests.

Chapter 3. Specimen Properties and Testing

3.1. Introduction

Test specimens used in this study were 5 portions of pretensioned T-beam specimens previously tested in the Auburn University Civil Engineering Department Structures Laboratory by Kelly Levy in 2006–2007 (Levy 2007). The original beams were 23'-0" long when cast and pretensioned. Each specimen tested in this study was one end of a beam that had been tested to failure in flexure. The resulting beam segments ranged in length from 129 in. to 148 in., and each had one undamaged end region that was a prestress transfer zone in the original beam. The cross section for all specimens is shown in Figure 3-1.

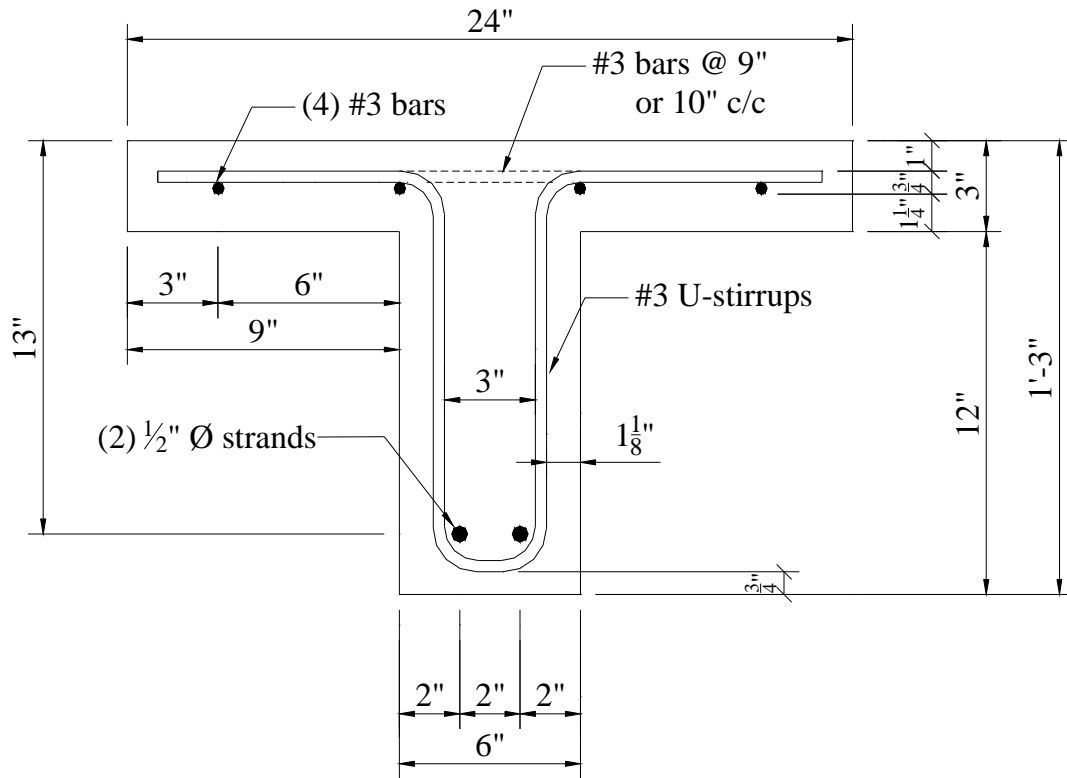


Figure 3-1. Specimen cross section detail (Levy 2007)

3.2. Specimen Identification

For ease of future reference, the specimen identification system is consistent with the system used by Levy (2007). Figure 3-2 shows the specimen identification scheme used by Levy.

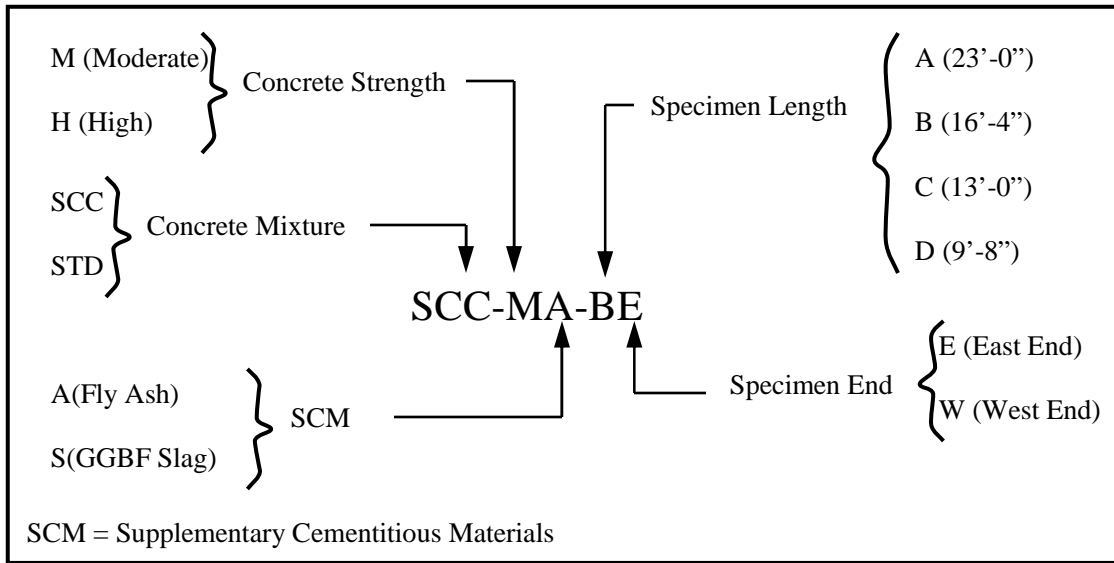


Figure 3-2. Specimen identification system of Levy (2007)

The modified identification system used for this study is shown in Figure 3-3. Not all the beams tested previously were available and appropriate for retesting. All of the beam portions came from the Length A beams of the previous study. The E or W descriptor represents whether the beam portion was the east or west end of the original flexural specimen. The beam portions that were used as specimens in this study were tested with a point load placed so that the undamaged prestress transfer end of the original beam was the short shear span. The S or L descriptor is used to differentiate between the two ends of the specimen as tested in this study.

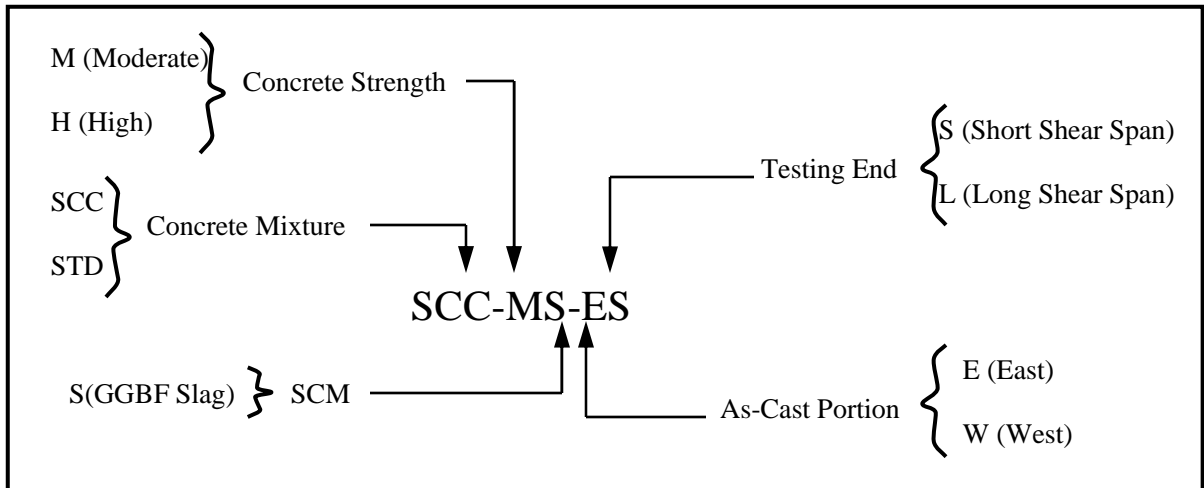


Figure 3-3. Specimen identification system used in this study

3.3. Material Properties

3.3.1. Prestressing steel

The prestressing steel used in this study was low-relaxation “½ in.–special” Grade 270 seven-wire prestressing strand. The cross-sectional area and modulus of elasticity of the strand given by the manufacturer are 0.164 in² and 28,900 ksi, respectively. The measured diameter of this strand was 0.515 in. The strand used in all of the beams came from one roll that was manufactured by the American Spring Wire Corporation.

3.3.2. Mild reinforcing steel

The mild reinforcing steel used in this study was ASTM A615 Grade 60 reinforcing bar. 0.375-in. nominal diameter No. 3 bars were used for flange reinforcement and transverse (shear) reinforcement. Transverse reinforcement was placed with 10 in. spacing. For analysis purposes, the modulus of elasticity and yield stress of the bars were assumed to be 29,000 ksi and 60 ksi, respectively.

3.3.3. Concrete

Three types of concrete mixtures were used in this study. One was a conventionally consolidated (“standard”) moderate-strength concrete mixture. The remaining two mixtures were self-consolidating concrete (SCC), one having high strength and one having moderate strength. The standard mixture was designed to resemble a mixture commonly used by the Alabama Department of Transportation (ALDOT) for prestressing applications.

The standard mixture is called STD-M (moderate-strength). The SCC mixtures used for this study were SCC-13 (high-strength) and SCC-15 (moderate-strength) using the notation of previous phases of this ALDOT project (Roberts 2005; Swords 2005). This study follows the Levy (2007) nomenclature, and the two SCC mixtures are called SCC-HS (high strength with GGBF slag), and SCC-MS (moderate strength with GGBF slag) respectively. The moderate-strength SCC mixture had a 50% Grade 100 GGBF slag replacement. The high-strength SCC mixture had a 30% Grade 100 GGBF slag replacement. All concrete mixtures had a maximum aggregate size of $\frac{3}{4}$ ". Mixture constituents, as well as fresh and hardened properties of the three concrete types, are given in Table 3-1, Table 3-2 and Table 3-3 as reported by Levy (2007):

Table 3-1. Mixture properties

Mixture Constituents	Mixtures		
	STD-M	SCC-MS	SCC-HS
Water (pcy)	270	270	260
Cement (pcy)	640	375	650
Fly Ash (pcy)	0	0	0
GGBF Slag (pcy)	0	375	279
Coarse agg. (pcy)	1964	1613	1544
Fine agg. (pcy)	1114	1323	1265
AEA (oz/cwt)	0.33	0.00	0.00
WRA (oz/cwt)	4.0	6.0	6.0
HRWRA (oz/cwt)	3.5	4.5	5.0
VMA (oz/cwt)	0.0	2.0	2.0

where:

GGBF = Ground Granulated Blast Furnace,

AEA = Air-Entraining Admixture,

WRA = Water-Reducing Admixture.

HRWRA = High-Range Water-Reducing Admixture, and

VMA = Viscosity-Modifying Admixture.

Table 3-2. Fresh properties

PROPERTY	MIXTURE		
	STD-M	SCC-MS	SCC-HS
Slump Flow (in.)	9.5	28.5	26
Unit Weight (lb/ft ³)	142.2	148.4	155.2
Air Content (%)	11.0	5.0	3.0
VSI	-	1.0	1.0
T-50 (sec.)	-	1.54	3.75
J-Ring Difference (in.)	-	2	2.5
L-Box (H ₂ /H ₁)	-	0.92	0.63
Temperature (°F)	82	89	95

Table 3-3. Hardened properties

PROPERTY	MIXTURE		
	STD-M	SCC-MS	SCC-HS
f'_{ci} (psi)	5000	5300	9990
$E_{c,i}$ (ksi)	4900	4950	6050
$f'_{c,28(ASM)}$ (psi)	5990	9640	13150
$f'_{c,28(AC)}$ (psi)	6320	9170	13380
$E_{c,28(AC)}$ (ksi)	5150	6950	7050
$f_{ct,28(AC)}$ (psi)	560	840	830

ASTM = Cured according to ASTM C192 specifications

AC = Air-cured

3.4. Prestressing Parameters

Several properties of the specimens related to prestressing steel were previously determined by Levy (2007). Transfer and development lengths ($l_{t,exp}$ and $l_{d,AASHTO}$, respectively), f_{pj} , f_{pe} and f_{ps} values for all five specimens are given in Table 3-4.

Table 3-4. Previous testing results

Specimen	$l_{t,exp}$ (in.)	$l_{d,AASHTO}$ (in.)	f_{pj} (ksi)	f_{pe} (ksi)	f_{ps} (ksi)
STD-M-E	22	75	209	178	264
STD-M-W	32	75	209	178	264
SCC-MS-E	20.5	72	211	188	265
SCC-HS-E	18	71	210	192	266
SCC-HS-W	20.5	71	210	192	266

where:

f_{pj} = stress in prestressing steel at jacking,

f_{pe} = effective stress in prestressing steel after losses, and

f_{ps} = average stress in prestressing steel at the time for which the nominal resistance of the member is required.

The transfer length, jacking stress, and effective stress values were determined based on measurements of concrete strains in the specimens. The development length and f_{ps} were determined using AASHTO LRFD design provisions.

3.5. Test Setup and Instrumentation

The test setup consisted of a simply supported beam loaded by a single concentrated load closer to the original prestress transfer end of the beam. The reason why unequal shear

spans were chosen was that shear failures were expected and longer embedment lengths were already tested by Levy (2007). Use of a nonsymmetric loading promoted failure at the undamaged, original prestress transfer end of the specimen. The test setup is illustrated in Figure 3-4, and a representative photograph is given in Figure 3-5.

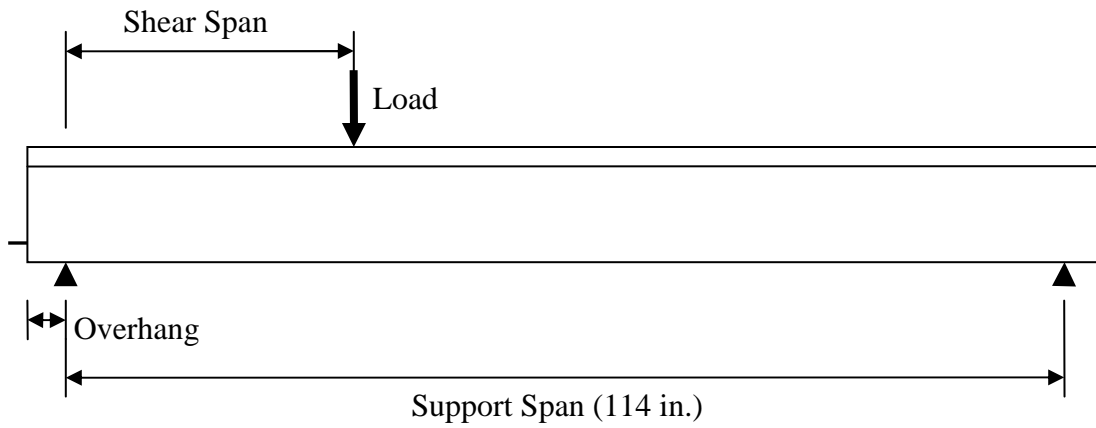


Figure 3-4. Test setup diagram



Figure 3-5 Test setup

For the Levy (2007) study, prestressing force was transferred by flame-cutting of the strands. Due to the physical orientation of the beams on the prestressing bed, each original beam had one flame-cut end and one dead end where strands were cut after the transfer. Table 3-5 indicates the physical differences of the test configuration for each specimen.

Table 3-5. Test configuration dimensions and strand release conditions

Specimen	Shear Span (in.)	Overhang (in.)	Strand Release Condition at End	Total Length (in.)
STD-M-E	30	4	Dead	129
STD-M-W	30	2	Flame Cut	148
SCC-MS-E	30	2	Dead	138
SCC-HS-W	30	2	Flame Cut	129
SCC-HS-E	16	2	Dead	147

Steel rocker supports were located at support positions and rested on reinforced concrete pedestals to elevate and support the specimens during testing. Between the steel supports and the specimen, lubricated and unreinforced neoprene pads were used to minimize horizontal force transfer. These supports can be seen in Figure 3-6.



Figure 3-6. Neoprene pads, steel supports and concrete blocks

Loading was applied by piston displacement of a hydraulic actuator attached to a reaction frame. Between the hydraulic piston and the beam there was a steel beam positioned to transmit the force to the load plate attached to the beam surface with a high strength gypsum-cement mixture. The hydraulic actuator may be seen in Figure 3-7.

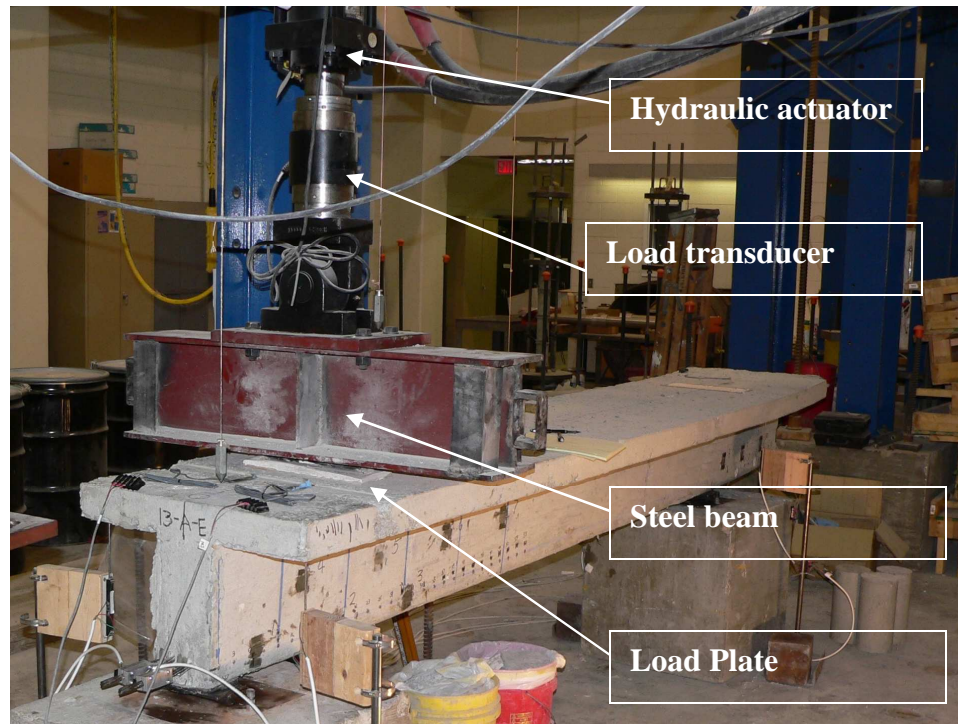


Figure 3-7. Hydraulic actuator and force transducer

3.6. Instrumentation

Applied load, displacements, top fiber compressive strains, and strand end slips were the main responses monitored during testing of specimens. Instruments used during the time of testing are presented in this section.

3.6.1. Measurement of applied load

The applied load was measured by a built-in force transducer between the hydraulic actuator and the steel beam. The force transducer and the steel beam can be seen in Figure 3-7.

3.6.2. Measurement of displacements

All displacements were measured using linear potentiometers. One potentiometer was placed under the beam directly below the load point. Potentiometers were also placed under the flange at each end on each face at the location of the support to measure any support deflection throughout each test. These potentiometers were also used as a safety measure to monitor any possible unexpected behavior of the beam under applied load. The actual displacement of the beam relative to the supports was calculated using the output from these potentiometers. Glass microscope slides were glued to the surface of the beam at the point of contact for each potentiometer in order to compensate for surface imperfections. Figure 3-8 show the positions of potentiometers used, and a close-up of two potentiometers can be seen in Figure 3.6.

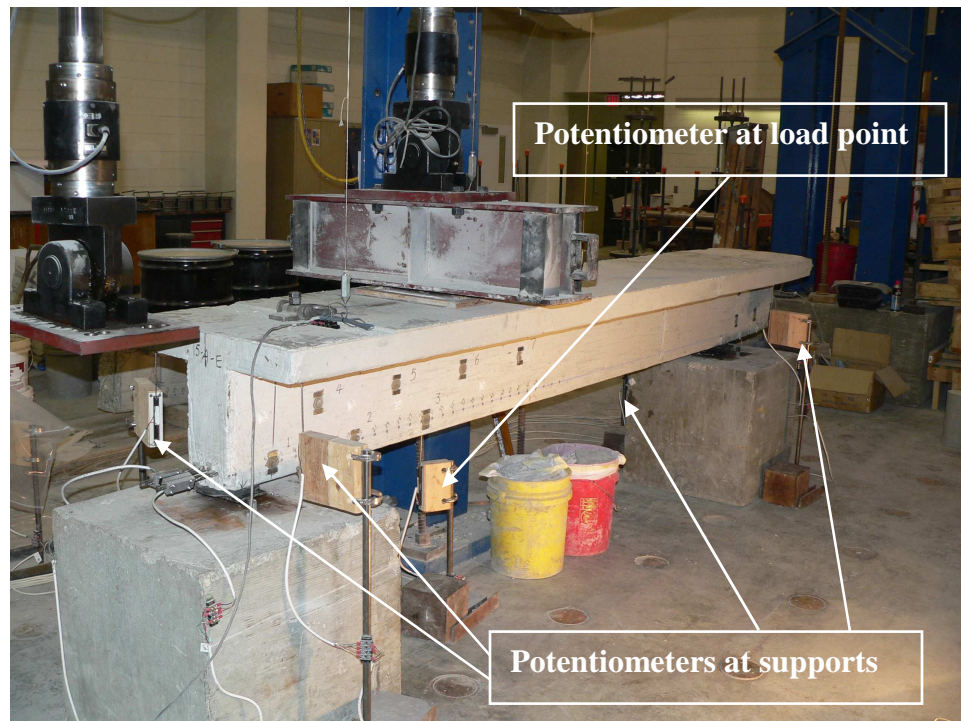


Figure 3-8. Potentiometers

3.6.3. Measurement of strand slip

Strand slip was measured with linear potentiometers at the end closest to the load point. This end, which was subjected to the larger shear force, was a prestress transfer location in the original beam. All strand movement was measured relative to the end of the beam. The potentiometers were mounted onto brackets which were then attached to the strands. Potentiometers used to measure strand slip can be seen in Figure 3-9.



Figure 3-9. Strand slip measurement

3.6.4. Measurement of strains at extreme compression fibers

Compressive strains at the top surface of the beam were monitored during flexural testing using an Electrical Resistance Strain Gauge (ERSG) with a 2.36-in. (60-mm) gauge length. For all specimens except SCC-HS-E, strain gauges were positioned 6 in. from the load point on the shorter shear span. For specimen SCC-HS-E, two strain gauges were

attached at the same distance but with 1 in. offsets from the centerline due to the presence of a recess for lifting hardware.

3.6.5. Data acquisition

All instrumentation signals were acquired by an Optim MEGADAC Data Acquisition/Signal Conditioning Unit and then transferred to a laptop computer where all data was recorded and stored. Data was acquired and stored every 1/10th of a second from each instrument. The data acquisition system used for testing is shown in Figure 3-10.



Figure 3-10. Data acquisition system

Chapter 4. Test Results

4.1. Introduction

This chapter includes a detailed description of each of the five tests in the experimental program. Key performance characteristics of all five tests are summarized at the end of the chapter.

4.2. Specimen STD-M-E

The applied load and strand slip versus load point displacement graph for specimen STD-M-E, constructed of a conventional moderate strength concrete mixture, is given in Figure 4-1.

After a range of approximately linear elastic behavior, a web-shear crack between the support and the load point was observed in specimen STD-M-E when the applied load reached 32.1 kips and the load point displacement was 0.05 in. The inclined shear crack that formed at this load is shown in Figure 4-2. Immediately after cracking, the width of the shear crack was about 0.5 mm (0.020 in.) at the prestressing strand level and 0.2 mm (0.008 in.) at the centroid of the cross section. The corresponding shear force when the crack opened was 23.6 kips. The cracking load was not attained again by the beam as more displacement was applied. After cracking, the specimen exhibited excessive strand slip which could also be heard at the time of experiment.

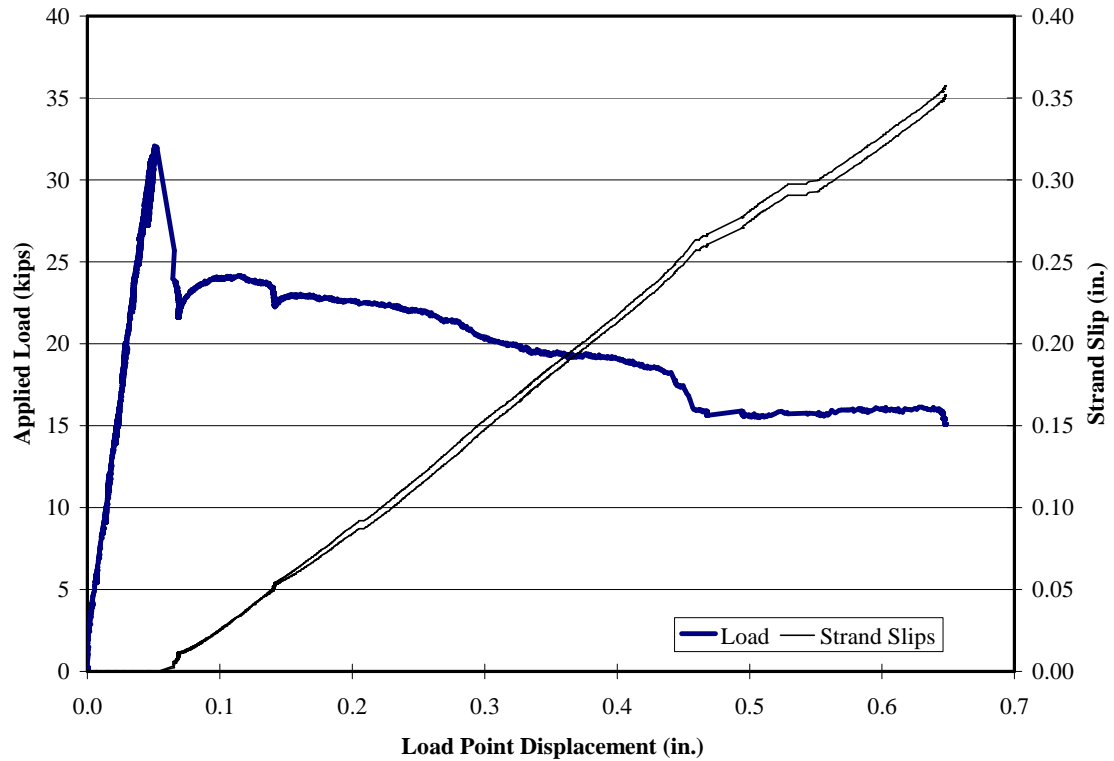


Figure 4-1. Applied load and strand slips vs. load point displacement - STD-M-E

A gradual failure of the specimen followed as the load point displacement was increased and the resistance of the beam decreased to a value of approximately 16 kips. The test was stopped at a displacement of 0.65 in. At this point, the crack width was 11 mm (0.43 in.) at the strand level and 4 mm (0.15 in.) at the centroid. Figure 4-3 and Figure 4-4 show the final state of the crack at the end of the test. The observed failure behavior was consistent with a “shear tension” failure, which (as related in Chapter 2) entails a loss of reinforcement development between the inclined crack and the beam end that is precipitated by the influence of a shear crack.



Figure 4-2. Initial crack at 32 kips applied load – STD-M-E

The shear crack was diagonally positioned 19 in. from the beam end at strand level, extending to 28 in. from beam end at the centroid.



Figure 4-3. Final state of crack at the end of test- STD-M-E



Figure 4-4. Shear tension failure showing loss of bond - STD-M-E

In order to have a better understanding of the behavior at the time of shear crack opening, a load point displacement and strand slip versus time graph, and an applied load and strand slip versus time graph are given in Figure 4-5 and Figure 4-6, respectively. Both graphs indicate that the shear crack and strand slip took place at the same 0.1-second data acquisition interval.

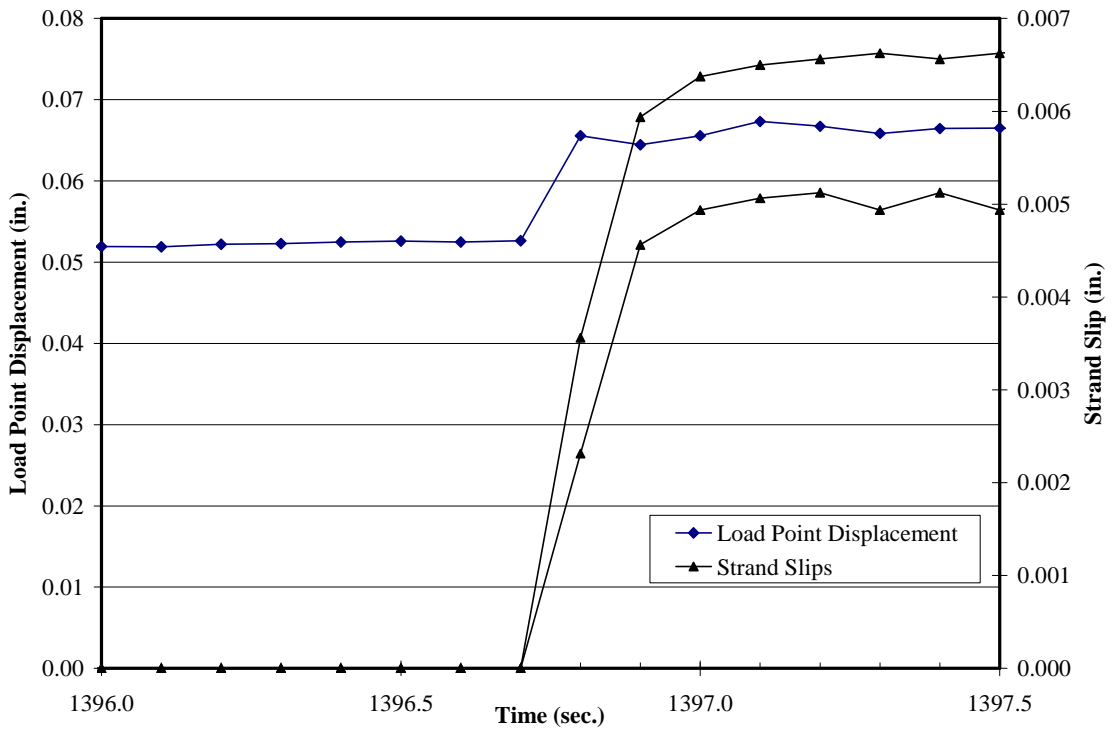


Figure 4-5. Load point displacement and strand slip versus time – STD-M-E

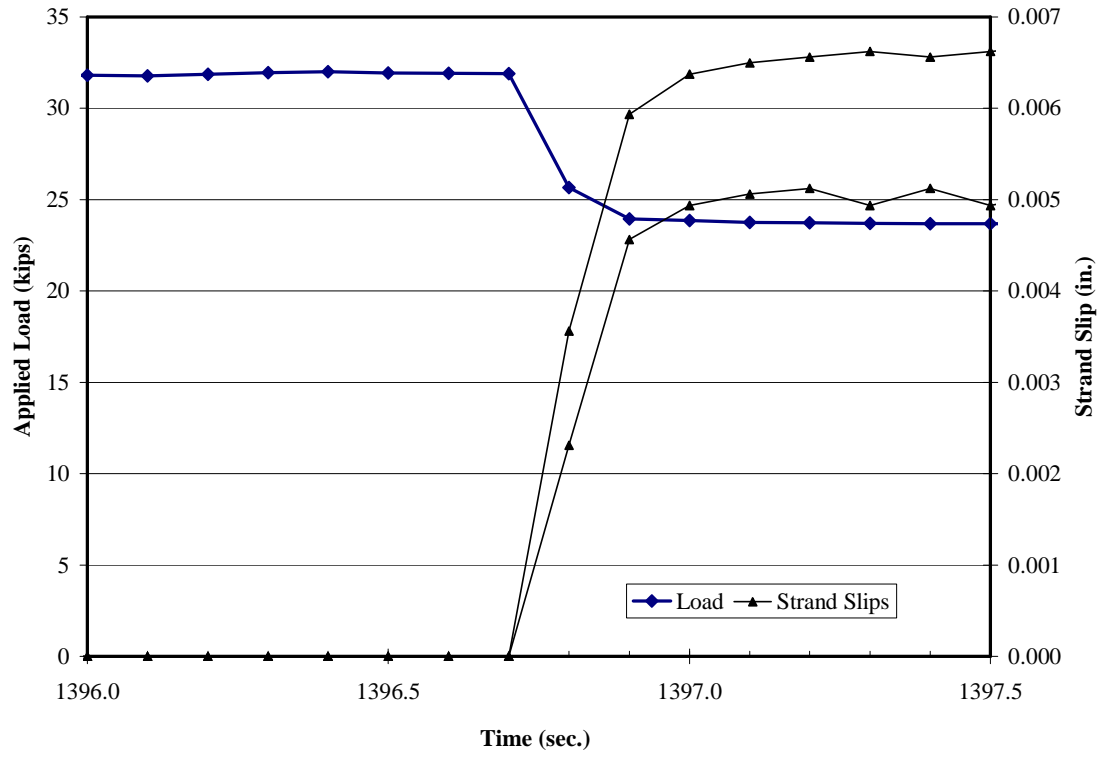


Figure 4-6. Applied load and strand slip versus time – STD-M-E

4.3. Specimen STD-M-W

The applied load and strand slip versus load point displacement graph of the specimen STD-M-W is given in Figure 4-7.

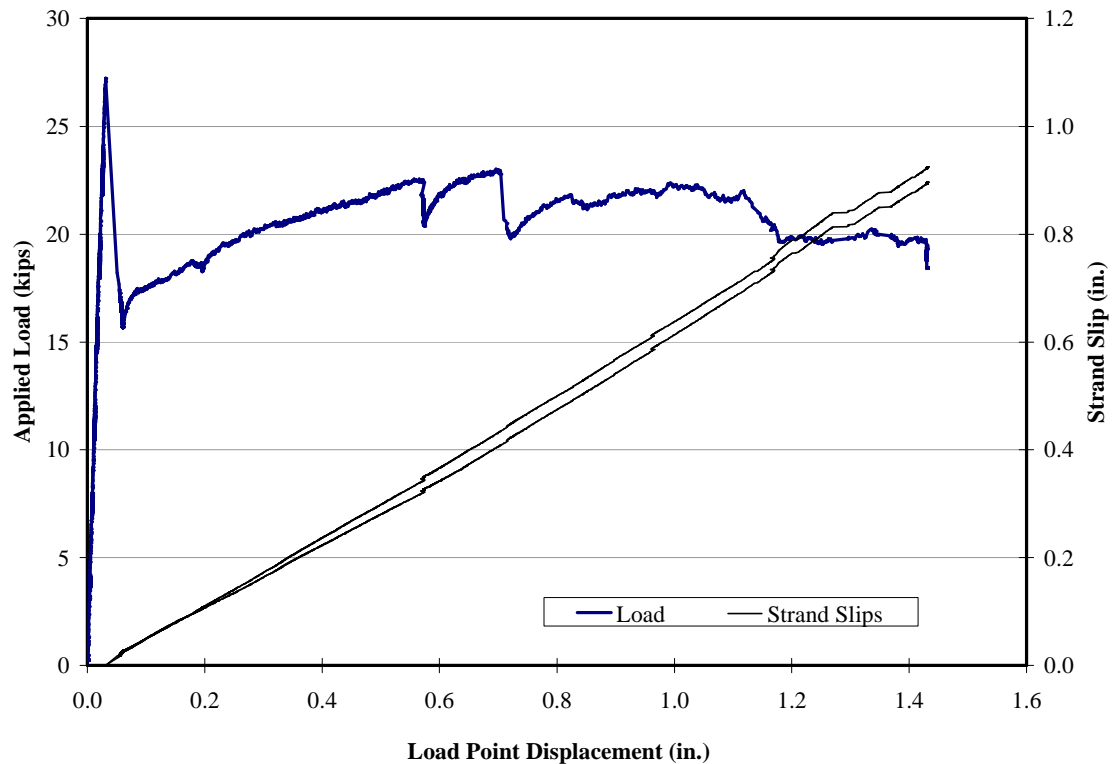


Figure 4-7. Applied load and strand slips versus load point displacement - STD-M-W

Behavior of STD-M-W was very similar to that of STD-M-E. Since they were portions of the same original beam, this was as expected. After a short range of linear elastic behavior, a web-shear crack between the support and the load point was observed at a 0.03 in. displacement, when the applied load reached 27.2 kips, lower than the cracking load of STD-M-E. This difference may be attributed to the longer transfer length in the short shear span of this specimen. The width of the shear crack was 0.6 mm (0.024 in.) at the prestressing strand level and 0.2 mm (0.008 in.) at the centroid. When the crack

opened, the corresponding shear force was 20.0 kips. This shear crack is shown in Figure 4-8. The cracking load could not be reached again, and the specimen exhibited excessive strand slip after this point. Again, a shear tension failure of the specimen followed as the displacement was increased. Finally, the crack width reached 8 mm (0.32 in.) at the strand level and 6 mm (0.24 in.) at the centroid. The test was stopped after 1.8 in. of displacement and 0.9 in. of strand slip. At this point, the load resisted by the beam was approximately 20 kips, and had remained fairly constant over the final 0.25 in. of displacement and 0.1 in. of strand slip. The final state of the specimen is shown in Figure 4-9.



Figure 4-8. STD-M-W: Initial crack at 27.2 kips applied load - STD-M-W

The shear crack was diagonally positioned 18 in. from the beam end at strand level, extending to 25 in. from the beam end at the centroid.



Figure 4-9. STD-M-W: Final state of crack at the end of test - STD-M-W

Load point displacement and strand slip versus time as well as applied load and strand slip versus time graphs of specimen STD-M-W are shown in Figure 4-10 and Figure 4-11. The behavior observed from these graphs is similar to that of STD-M-E, showing the same simultaneous behavior of shear crack opening and strand slip.

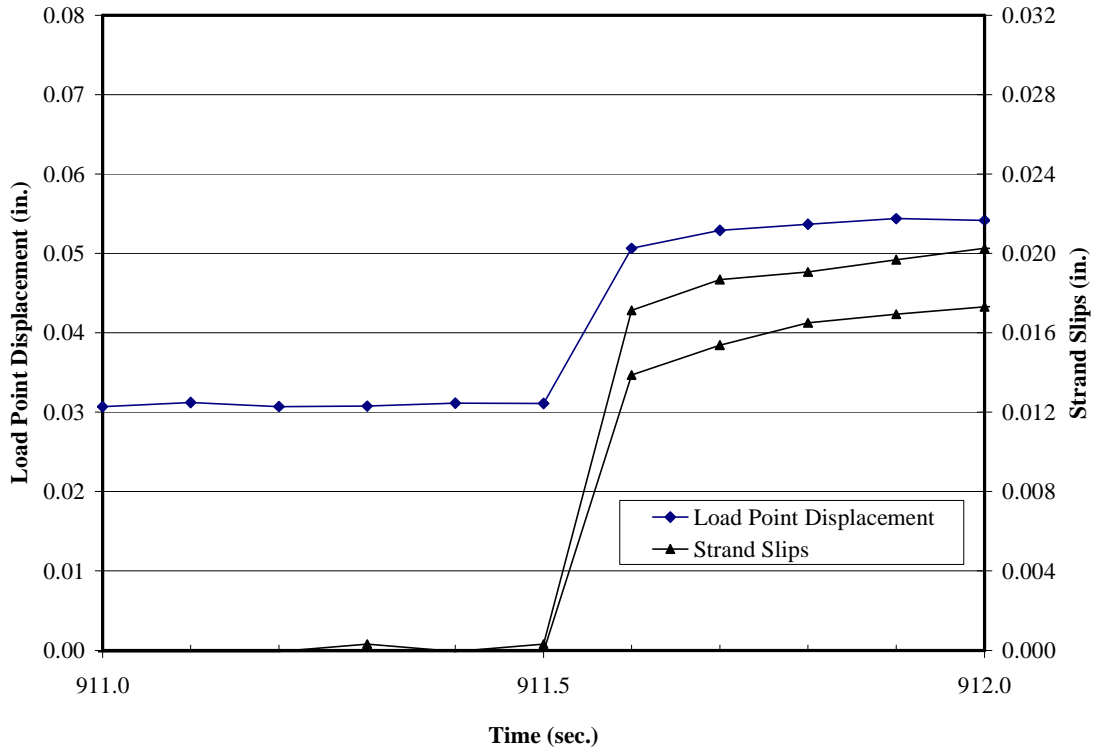


Figure 4-10. Load point displacement and strand slip versus time - STD-M-W

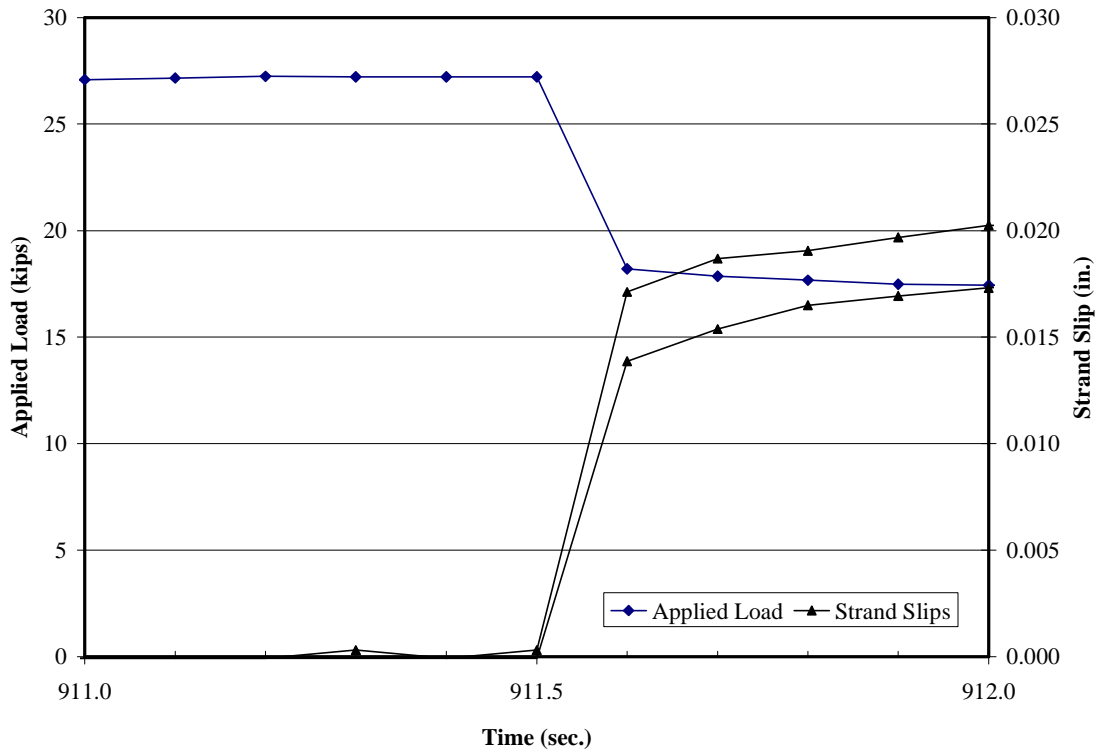


Figure 4-11. Applied load and strand slip versus time - STD-M-W

4.4. Specimen SCC-MS-E

The applied load and strand slip versus load point displacement graph of specimen SCC-MS-E is given in Figure 4-12.

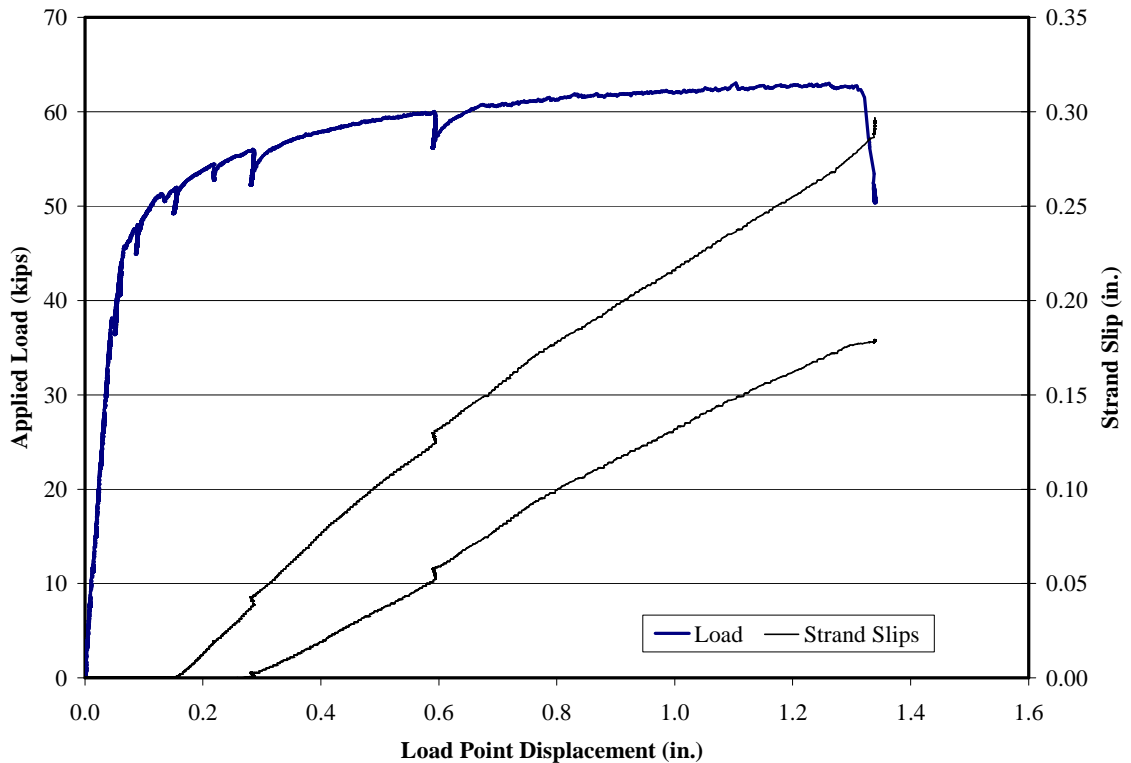


Figure 4-12. Applied load and strand slips versus load point displacement - SCC-MS-E

Specimen SCC-MS-E exhibited a different behavior when compared to the standard concrete specimens. This specimen did not have a shear crack but it had flexural cracks under the load point, which can be seen in Figure 4-13 and Figure 4-14. The applied load at first cracking was 46.1 kips, and the specimen failed in a flexural failure mode after opening of several flexural cracks reaching a maximum load of 63.1 kips. Figure 4-15 and Figure 4-16 show the state of the flexural cracks and the beam at the end of testing. Strand slips initiated when the flexural crack started to get wider at 51.7 kips of applied load. Although strand slip gradually increased with increasing load, strand

anchorage was sufficient to allow the strands to rupture in tension at a load of 63.1 kips. The width of the main crack at strand level was recorded as 1.5 mm (0.060 in.) at 56 kips and 11 mm (0.43 in.) at the end of the test.

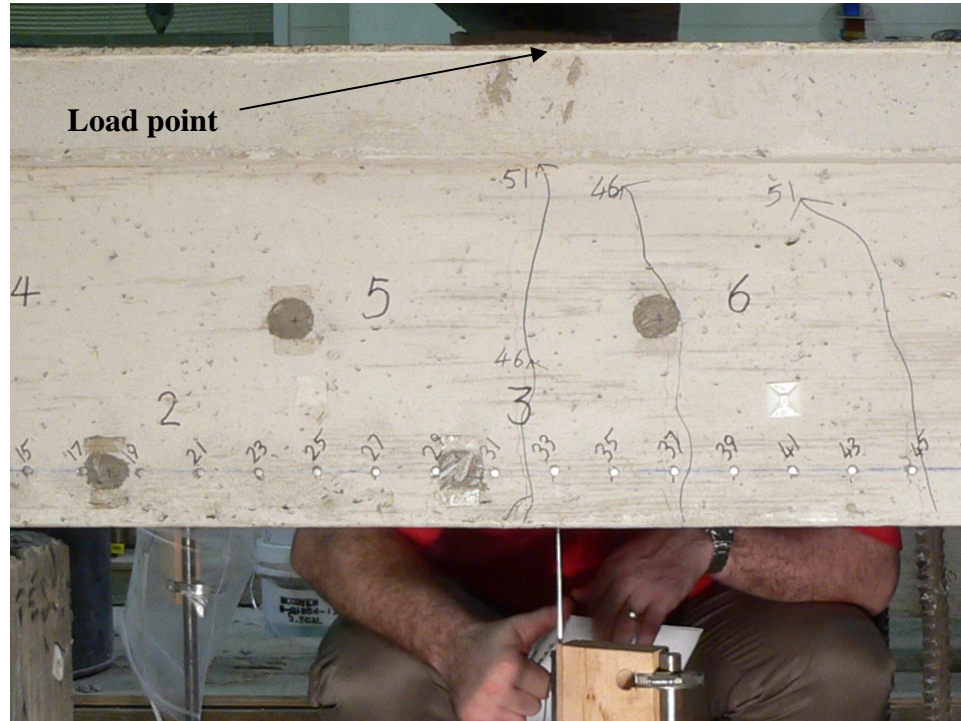


Figure 4-13. Flexural cracks under load point at 51 kips applied load - SCC-MS-E

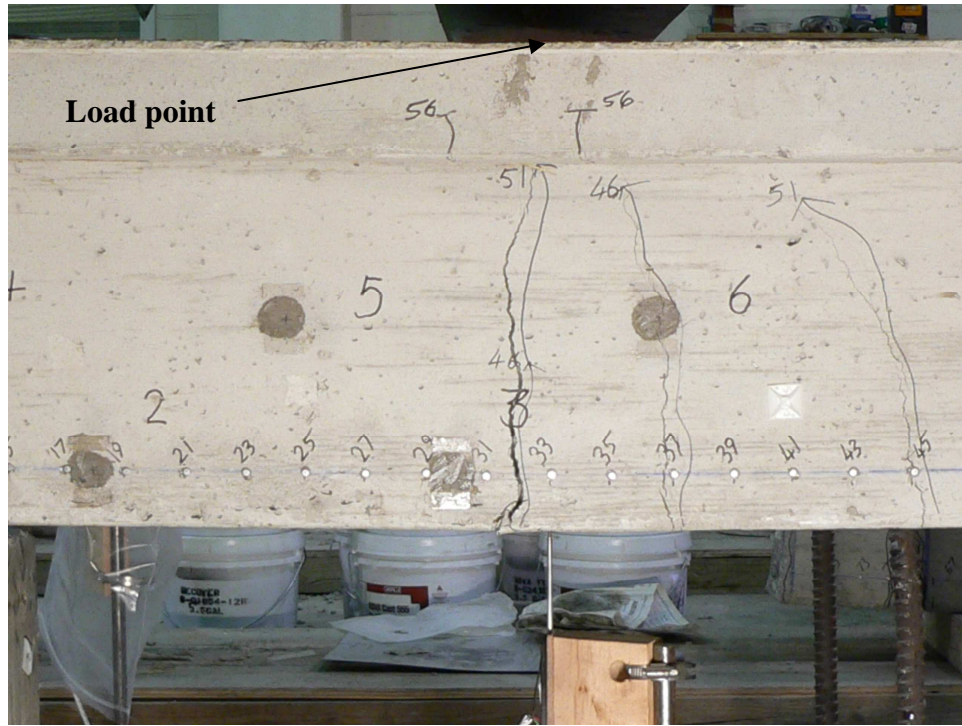


Figure 4-14. Flexural cracks under load point at 56 kips applied load - SCC-MS-E

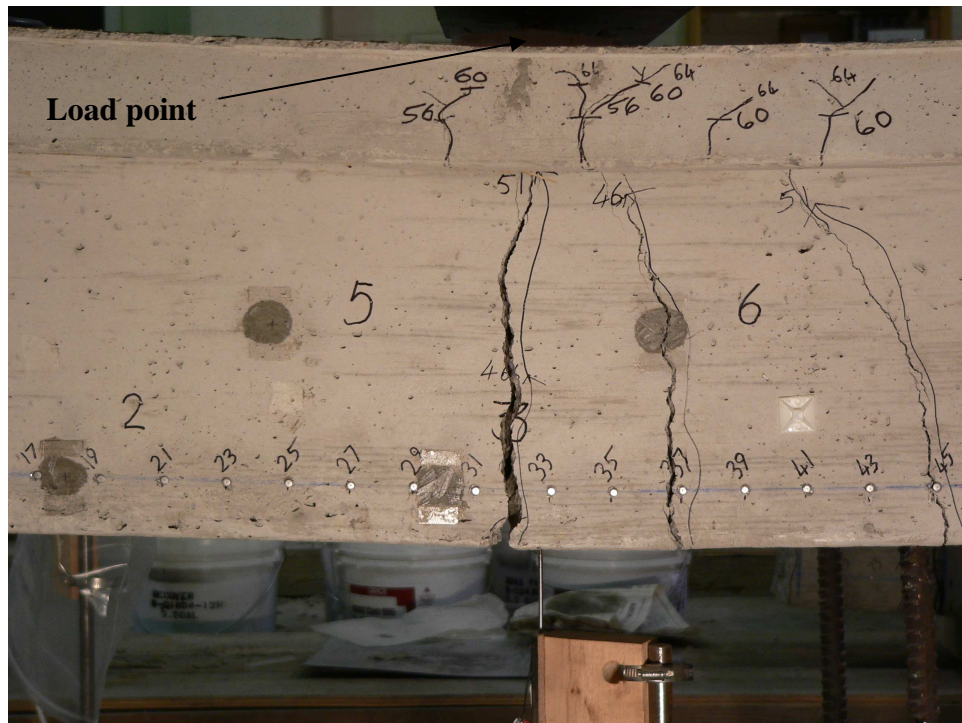


Figure 4-15. Final condition of flexural cracks at the end of test - SCC-MS-E



Figure 4-16. Final condition at the end of test - SCC-MS-E

4.5. Specimen SCC-HS-W

The applied load and strand slip versus load point displacement graph for specimen SCC-HS-W is given in Figure 4-17.

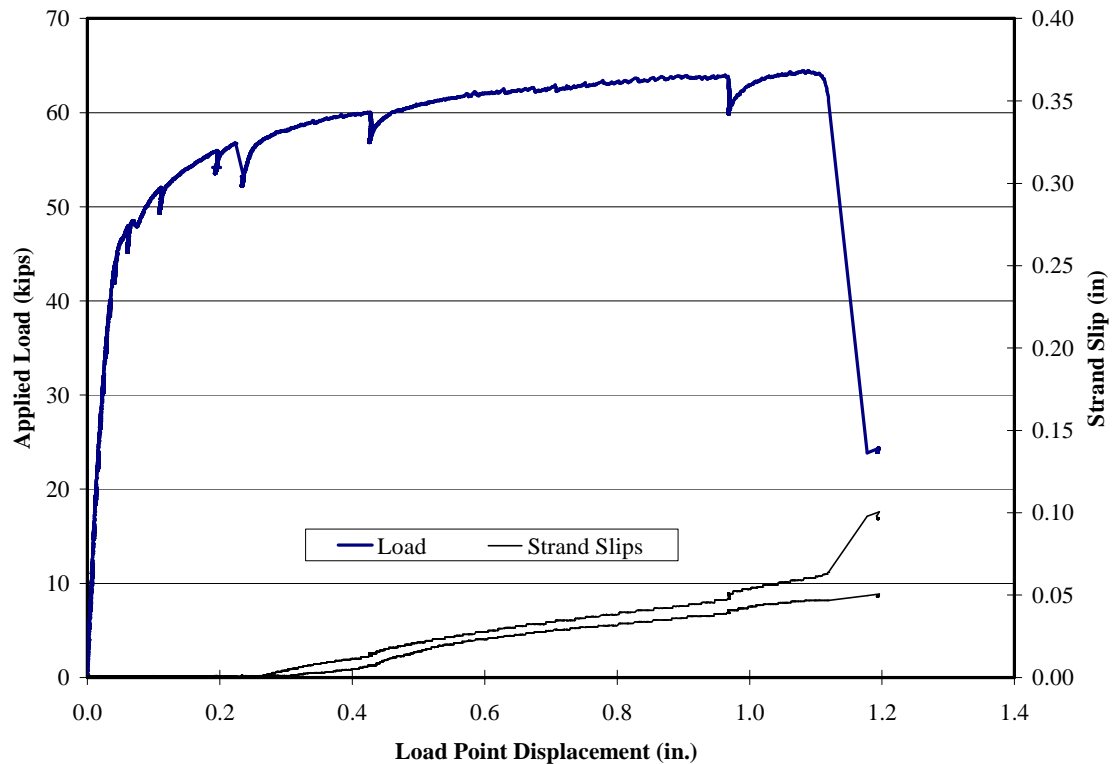


Figure 4-17. Applied load and strand slips versus load point displacement - SCC-HS-W

Specimen SCC-HS-W had behavior similar to the moderate-strength SCC specimen SCC-MS-E. Again, this specimen did not have a shear crack, but it had flexural cracks under the load point. The initial crack is shown in Figure 4-18. Cracking initiated at an applied load of 46.6 kips, and the specimen failed in a flexural failure mode after opening of several flexural cracks, reaching a maximum load of 64.5 kips when the strands ruptured. Strand slips initiated at 56.7 kips of applied load. However, strand slips in this specimen were not as large as in the previous tests. The width of the main crack at

strand level was recorded as 1.0 mm (0.040 in.) at 56 kips and 8 mm (0.32 in.) at the end of the test, just before the strands ruptured. The final state of flexural cracks and the beam are shown in Figure 4-19 and Figure 4-20.

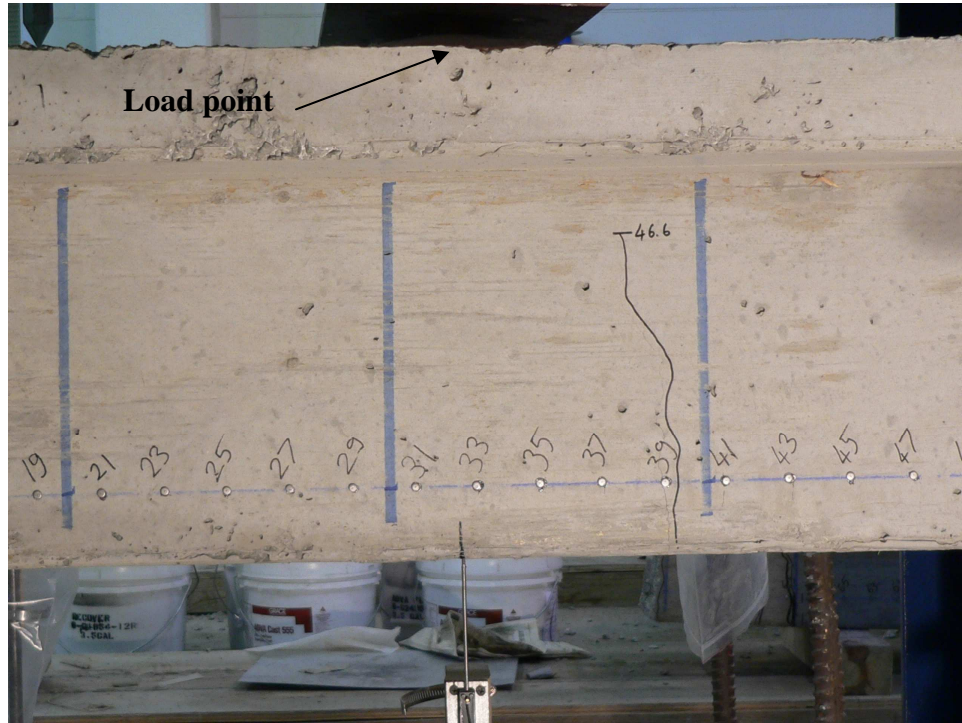


Figure 4-18. Flexural cracks under load point at 48 kips applied load - SCC-HS-W

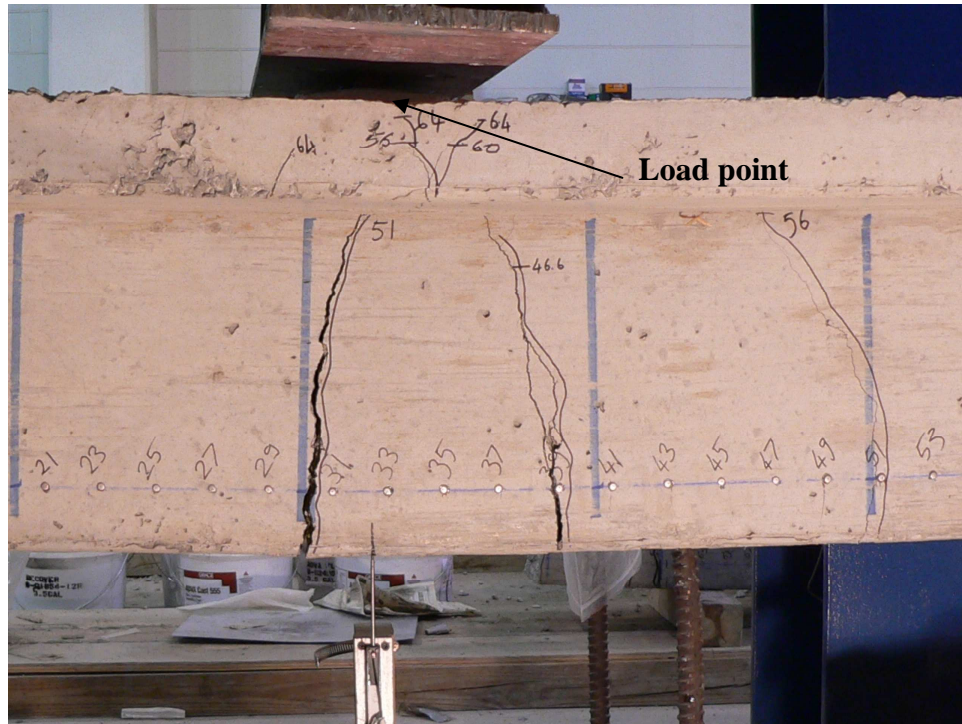


Figure 4-19. Final condition of flexural cracks at the end of test - SCC-HS-W



Figure 4-20. Final condition at the end of test - SCC-HS-W

4.6. Specimen SCC-HS-E

The applied load and strand slip versus load point displacement graph for specimen SCC-HS-E is given in Figure 4-21. This specimen came from the same original beam as specimen SCC-HS-W; however, the shear span was reduced to 16 in. (See Table 3-5 for test configuration dimensions.)

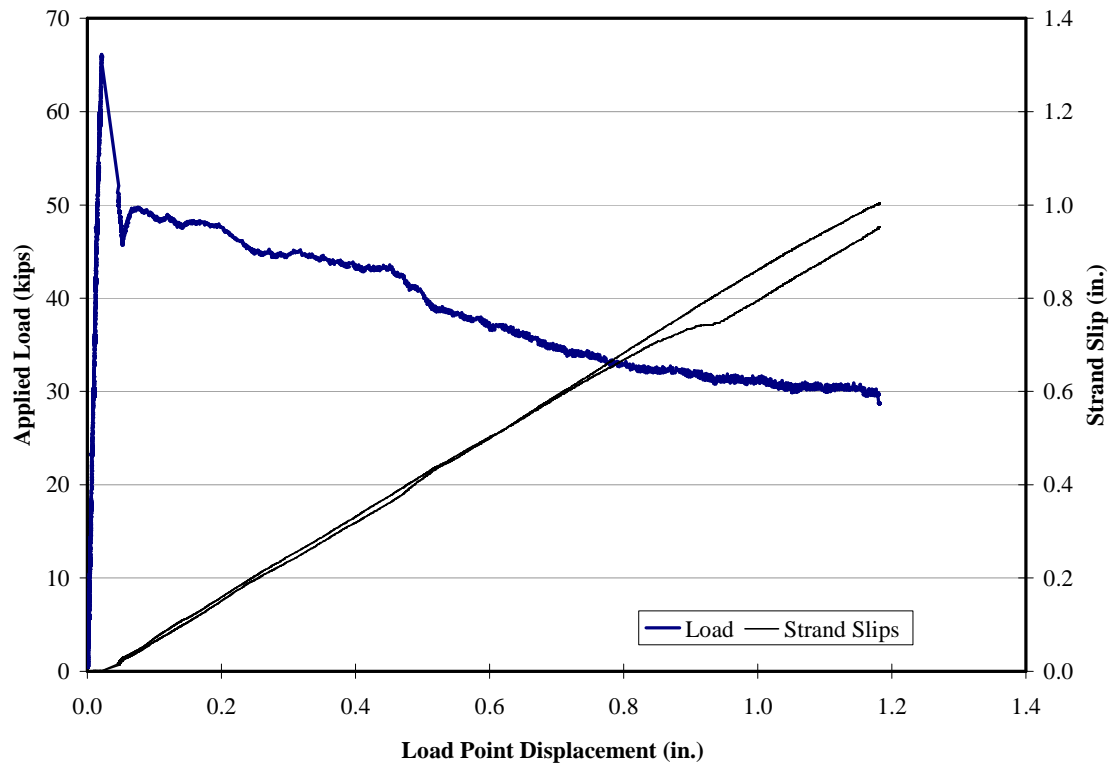


Figure 4-21. Applied load and strand slips versus load point displacement - SCC-HS-E

Specimen SCC-HS-E exhibited a similar behavior as the moderate-strength concrete specimens with longer shear spans (and longer effective strand embedment lengths). After a range of elastic behavior, a web-shear crack between the support and the load point was observed in the specimen when the applied load reached 66.1 kips. This shear crack can be observed in Figure 4-22. At this load, the width of the shear crack was 0.8 mm (0.032 in.) at prestressing strand level and 0.3 mm (0.012 in.) at the centroid of

the cross section. The shear force when the crack opened was 56.8 kips. This shear is a higher percentage of the applied load (86%) than in the rest of the test specimens (74%) because of the shorter shear span for this test.

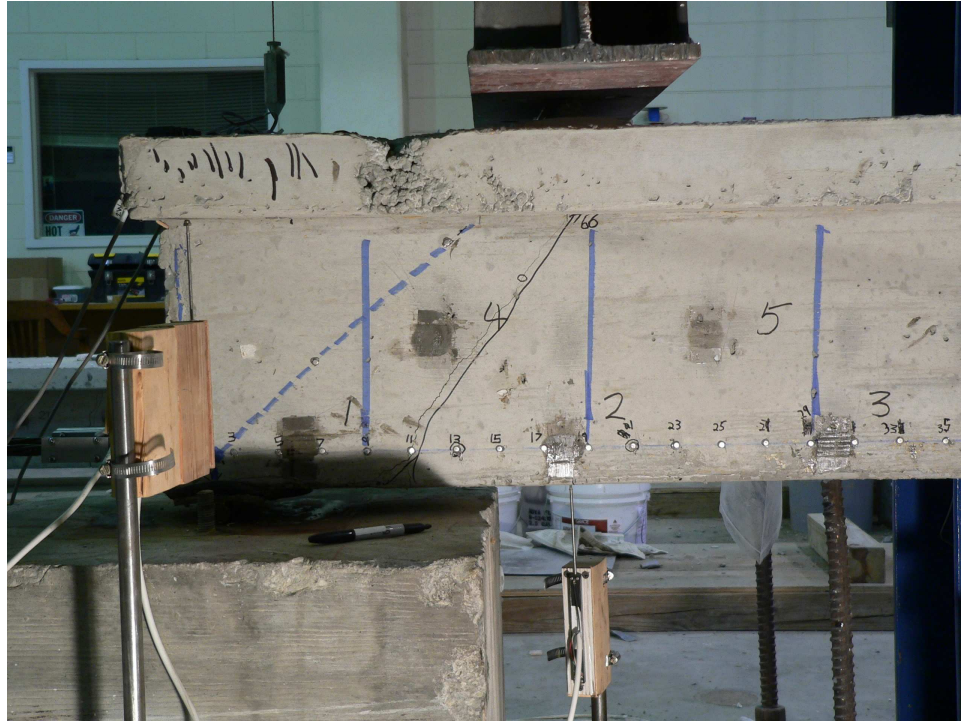


Figure 4-22. Shear crack at 66 kips cracking load - SCC-HS-E

After cracking, the specimen exhibited excessive strand slip, and the cracking load could not be reached again as a shear tension failure of the specimen was evident as the load point displacement was increased. Finally, the test was stopped at a displacement of 1.2 in. and an applied load of 30 kips. At this point, the crack width had reached 35 mm (1.38 in.) at strand level and 11 mm (0.43 in.) at the centroid. Strand slips had increased to approximately 1.0 in. at the cessation of the test. Figure 4-23 shows the final state of the shear crack at the end of test.

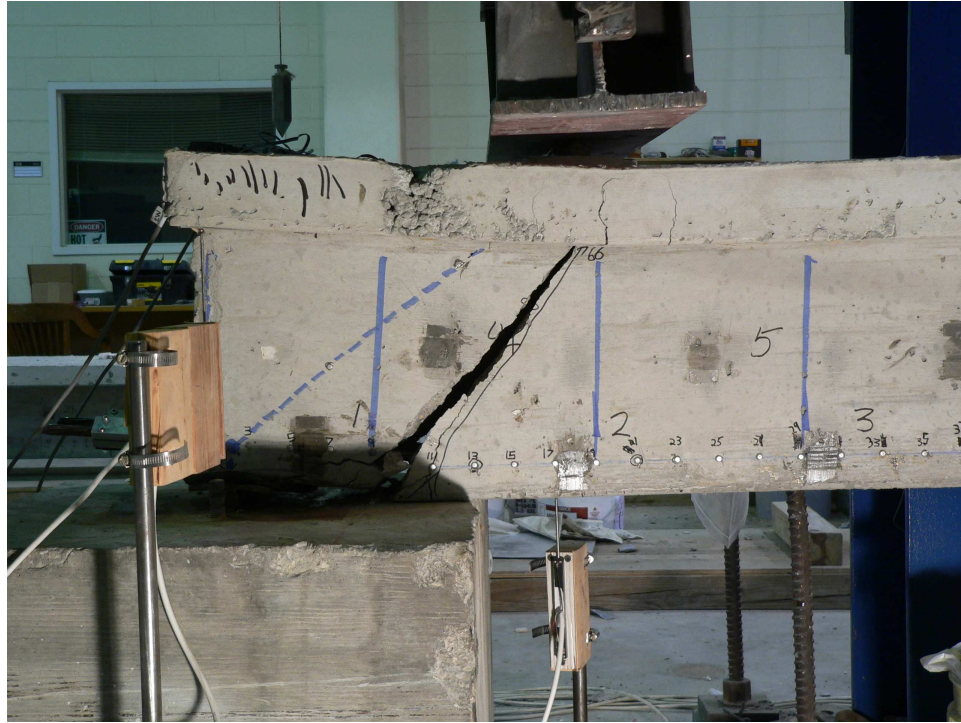


Figure 4-23. Final state of the shear crack at the end of test - SCC-HS-E

The shear crack was diagonally positioned 11 in. from beam end at strand level extending to 18 in. from the beam end (directly below the load point) at the centroid.

Load point displacement and strand slip versus time and applied load and strand slip versus time graphs of specimen SCC-HS-E are shown in Figure 4-24 and Figure 4-25. Behavior observed from these graphs is similar to those of moderate-strength, conventionally consolidated concrete specimens STD-M-E and STD-M-W, showing the same simultaneous behavior of shear crack opening and strand slip.

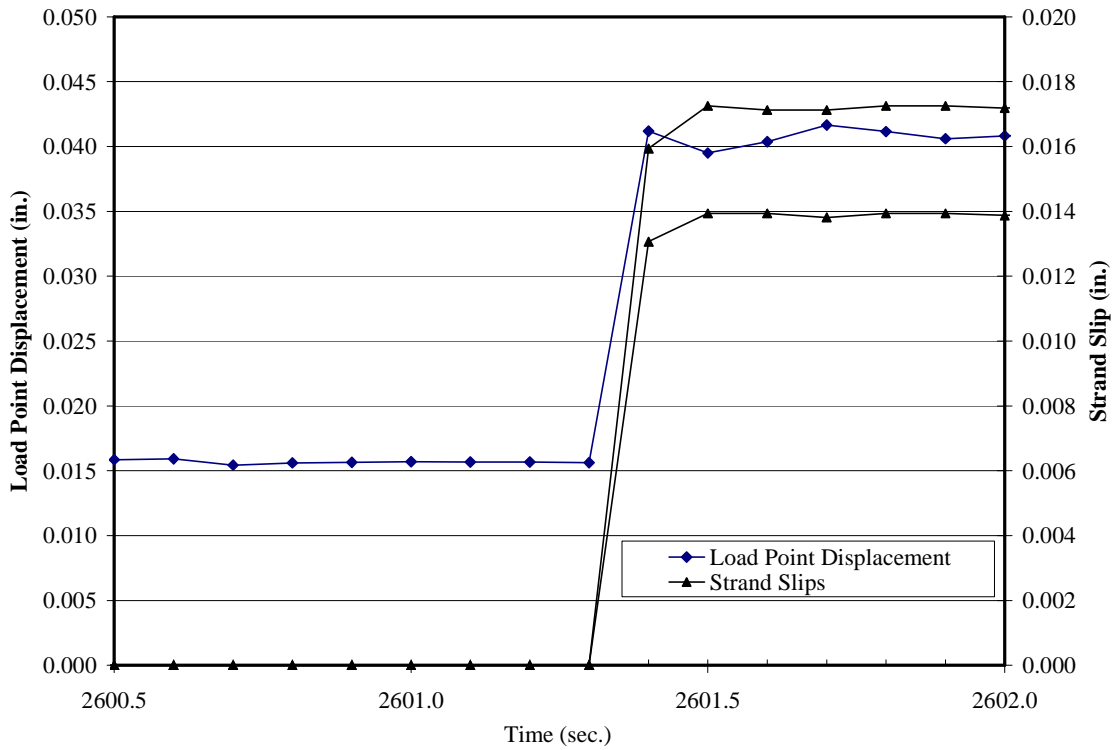


Figure 4-24. Load point displacement and strand slip versus time - SCC-HS-E

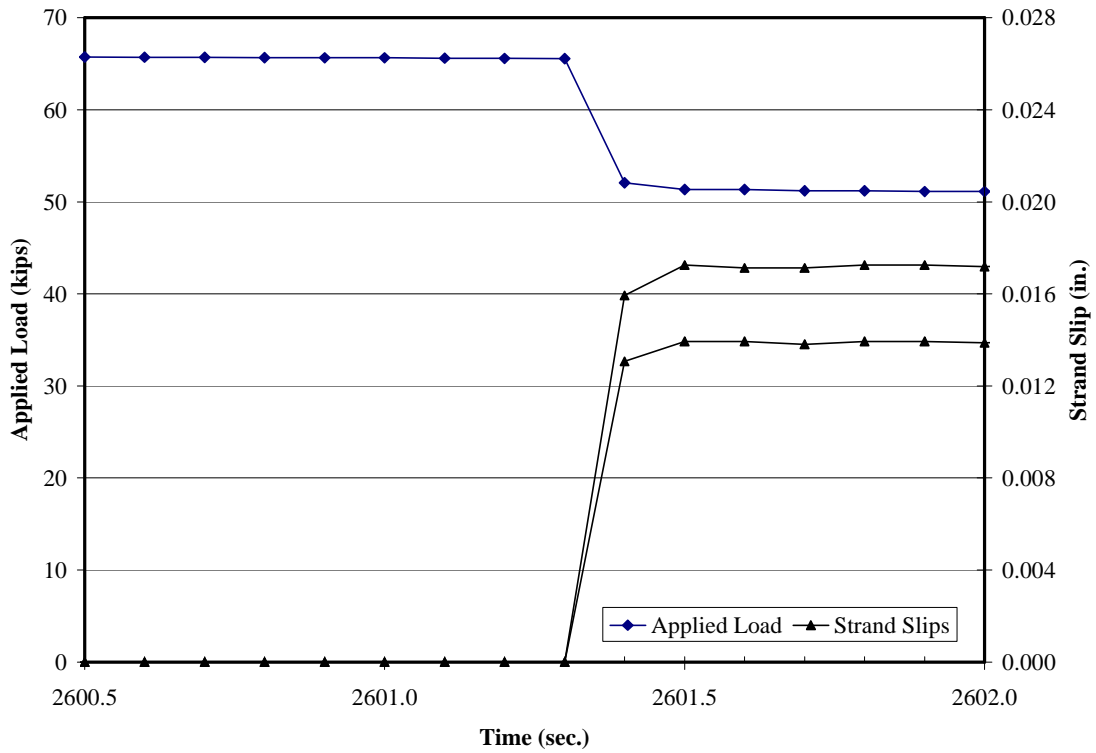


Figure 4-25. Applied load and strand slip versus time - SCC-HS-E

4.7. Summary of Test Results

Table 4-1 is provided to show a summary of cracking loads, ultimate loads, types of cracks and failure modes. Further analyses, comparisons and related discussions follow in Chapter 5.

Table 4-1. Specimen cracking and ultimate loads and failure modes

Specimen	Shear span (in.)	Cracking load (kips)	Ultimate load (kips)	Type of crack	Failure mode
STD-M-E	30	32.1 (23.6)	32.1 (23.6)	Web-shear	Shear-tension
STD-M-W	30	27.2 (20.0)	27.2 (20.0)	Web-shear	Shear-tension
SCC-MS-E	30	48.1 (35.4)	63.1 (46.5)	Flexural	Flexural/Strand slip
SCC-HS-W	30	48.0 (35.4)	64.5 (47.5)	Flexural	Flexural/Strand slip
SCC-HS-E	16	66.1 (56.8)	66.1 (56.8)	Web-shear	Shear-tension
Corresponding shear forces are given in parentheses					

Table 4-2 shows the initial crack positions of the specimens with respect to beam ends and support points. Crack position is given at strand level and at centroid.

Table 4-2. Crack positions of specimens

Specimen	At strand level (in.)	At centroid (in.)	Type of crack
STD-M-E	19	28	Web-shear
STD-M-W	18	25	Web-shear
SCC-MS-E	32	32	Flexural
SCC-HS-W	39	38	Flexural
SCC-HS-E	11	18	Web-shear

Chapter 5. Analysis and Discussion

5.1. Flexural Analysis

It can be seen from the test results that three test specimens (STD-M-E, STD-M-W and SCC-HS-E) failed with shear-tension modes of failure, and the remaining two (SCC-MS-E and SCC-HS-W) beams exhibited flexural modes of failure.

A layer-by-layer flexural analysis, as described by Collins and Mitchell (1997), was performed for each of the specimens in order to evaluate their idealized flexural response, ignoring the effects of shear deformations. The beam cross section was divided into several thin layers with unequal thicknesses which were analyzed as individual members being subjected to axial loading. The relative deformations of these layers were constrained so that plane sections remained plane. A total of forty-one layers were implemented, with thinner layers in the flange of the beam—where inelastic compressive behavior was expected—and thicker layers in the web region. The rows of mild steel reinforcement and prestressing strand were represented by two additional layers. The subdivision of each cross section into layers is shown in Figure 5-1. An elastic uncracked analysis was used to estimate initial stresses and strains for each layer.

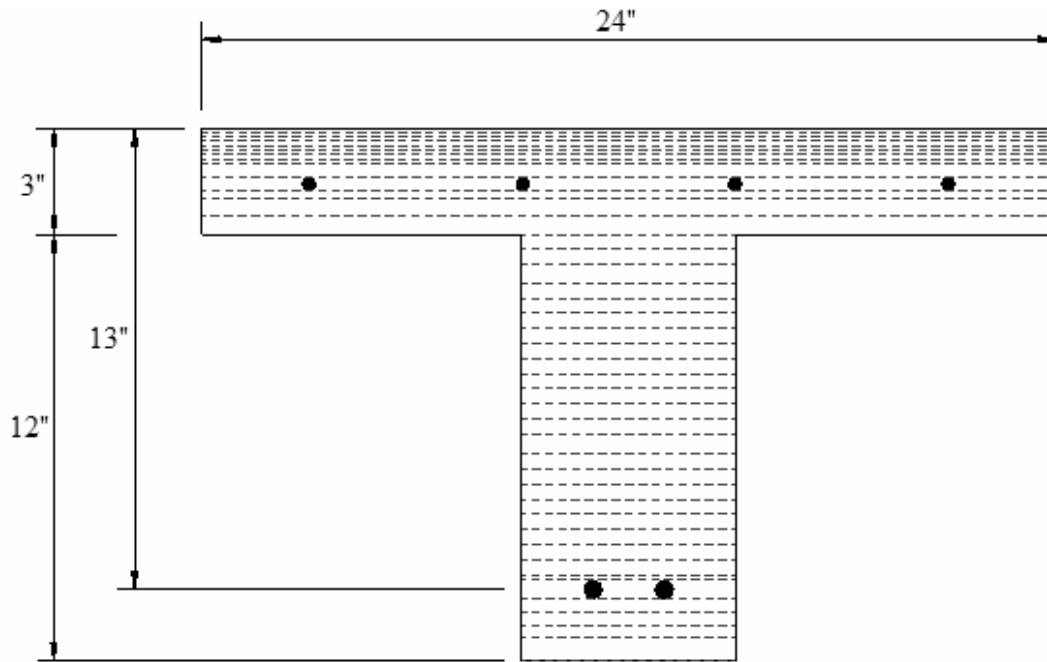


Figure 5-1. Layers for sectional analysis

For each value of top fiber compressive strain, the corresponding neutral axis depth and curvature were calculated based on an initial guess, followed by iteration aimed to zero the sum of axial forces of all of the layers. After the neutral axis location and curvature were determined, the corresponding value of moment was calculated. This procedure was repeated for a range of top fiber strains from a dead-weight only condition to ultimate flexural capacity.

For prediction of load-displacement response, tension stiffening was considered based upon the procedure described by Collins and Mitchell (1997). After cracking, concrete fibers located within 7.5 diameters of reinforcement were assigned average tensile stresses according to the relationship described by Collins and Mitchell (1997). 28th day air-cured compressive and tensile strengths of concrete are used as given in Table 3-3. Figure 5-2 shows the zones of concrete fibers affected by tension stiffening.

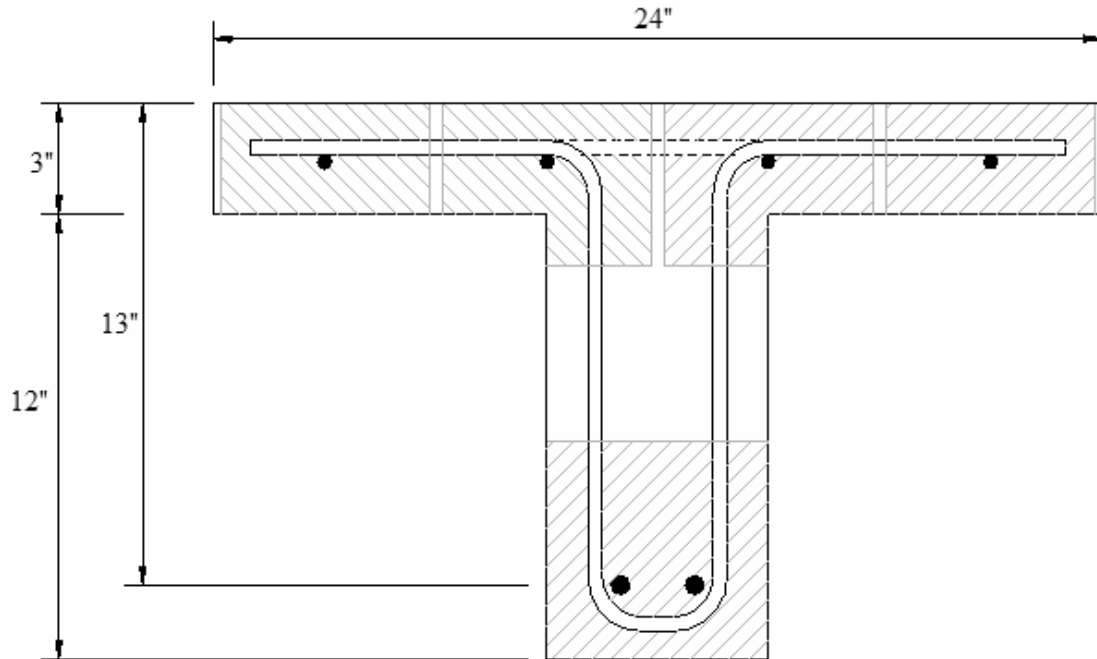


Figure 5-2. Concrete fibers affected by tension stiffening

Mild reinforcing steel was assumed linear elastic up to a yield point of 61 ksi with $E_s = 29,000$ ksi (determined according to previous material testing). Beyond the yield point a perfectly plastic behavior (constant stress) was assumed.

For the prestressing strands the following relationship was used based on previous material testing:

$$f_p = \varepsilon_p \left(959.48 + \frac{27941}{(1 + (114\varepsilon_p)^{12})^{1/12}} \right)$$

where,

f_p = stress in prestressing steel, and

ε_p = strain in prestressing steel.

Applied load versus load-point deflection graphs for all five specimens are given in Figure 5-3 through Figure 5-7, showing comparisons of calculated idealized flexural response with the actual experimental response. Calculated and measured flexural cracking and ultimate loads for each specimen are given in Table 5-1. The applied load that corresponds to the AASHTO nominal moment capacity is also reported in this table. This load is less than the value computed from the layer-by-layer approach because AASHTO limits the stress in the strands to a value less than the nominal strength of 270 ksi.

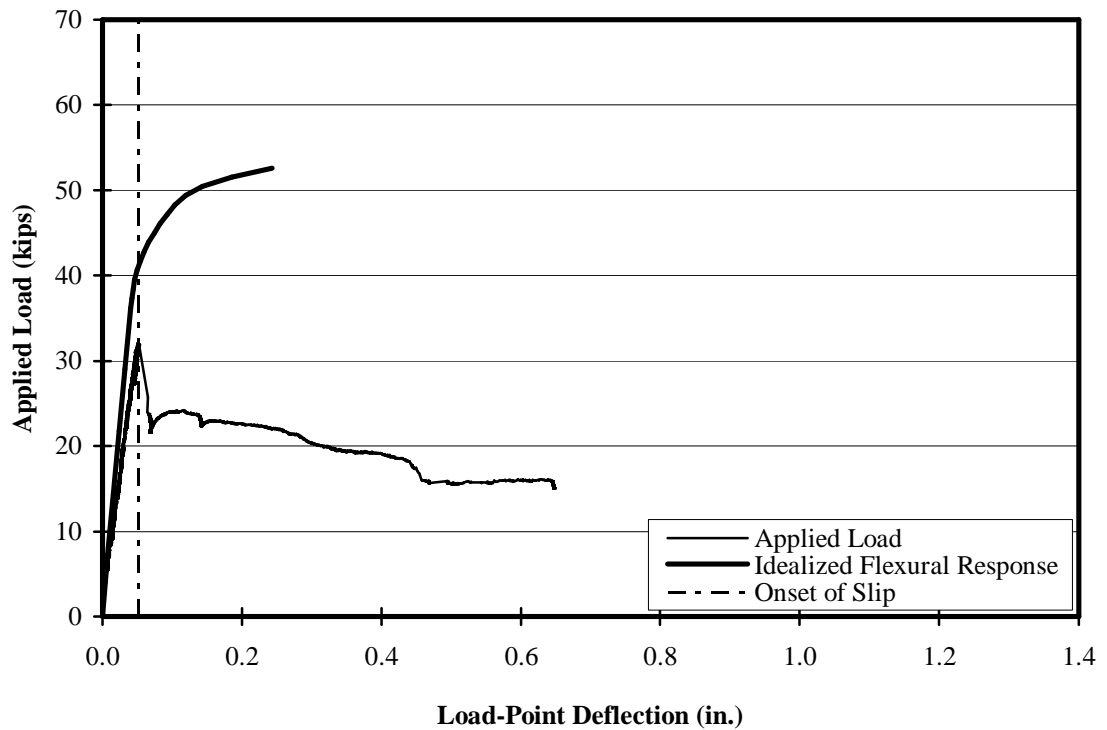


Figure 5-3. Flexural analysis result for STD-M-E

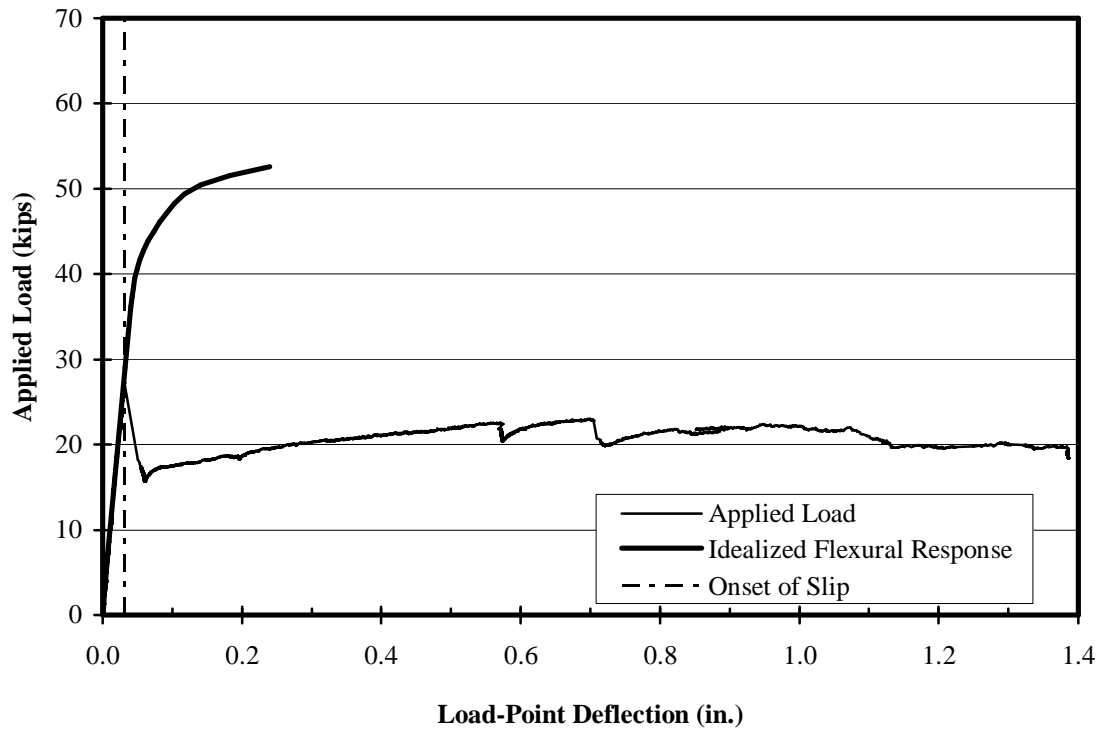


Figure 5-4. Flexural analysis result for STD-M-W

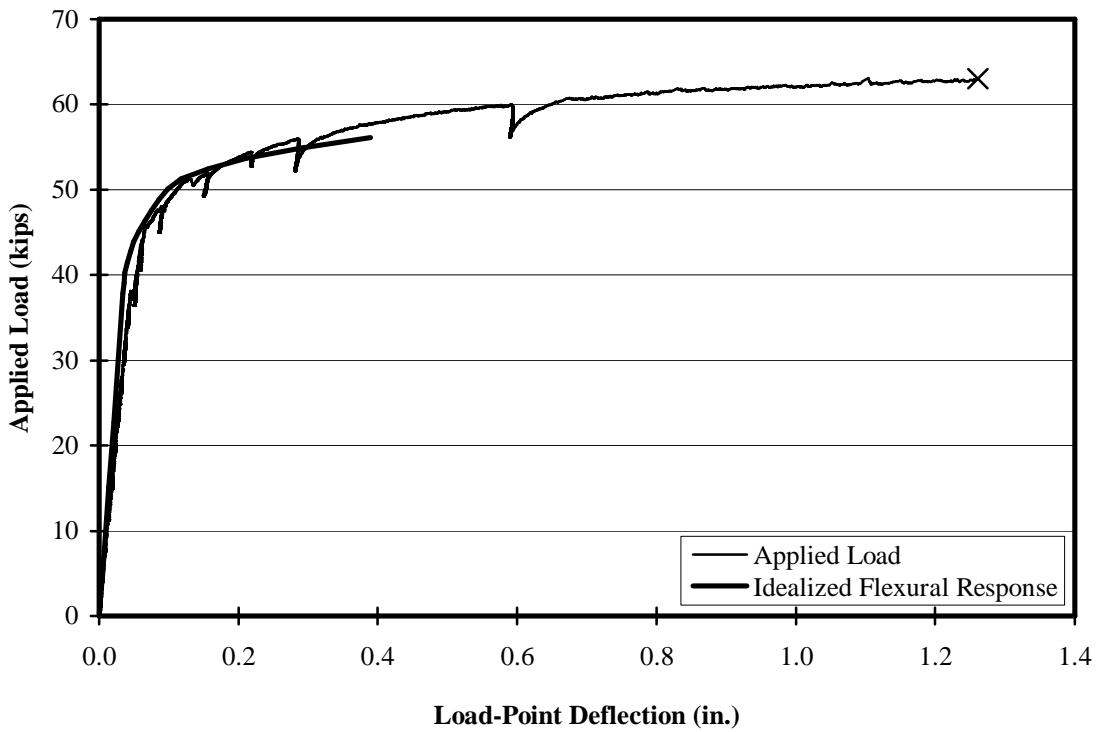


Figure 5-5. Flexural analysis result for SCC-MS-E

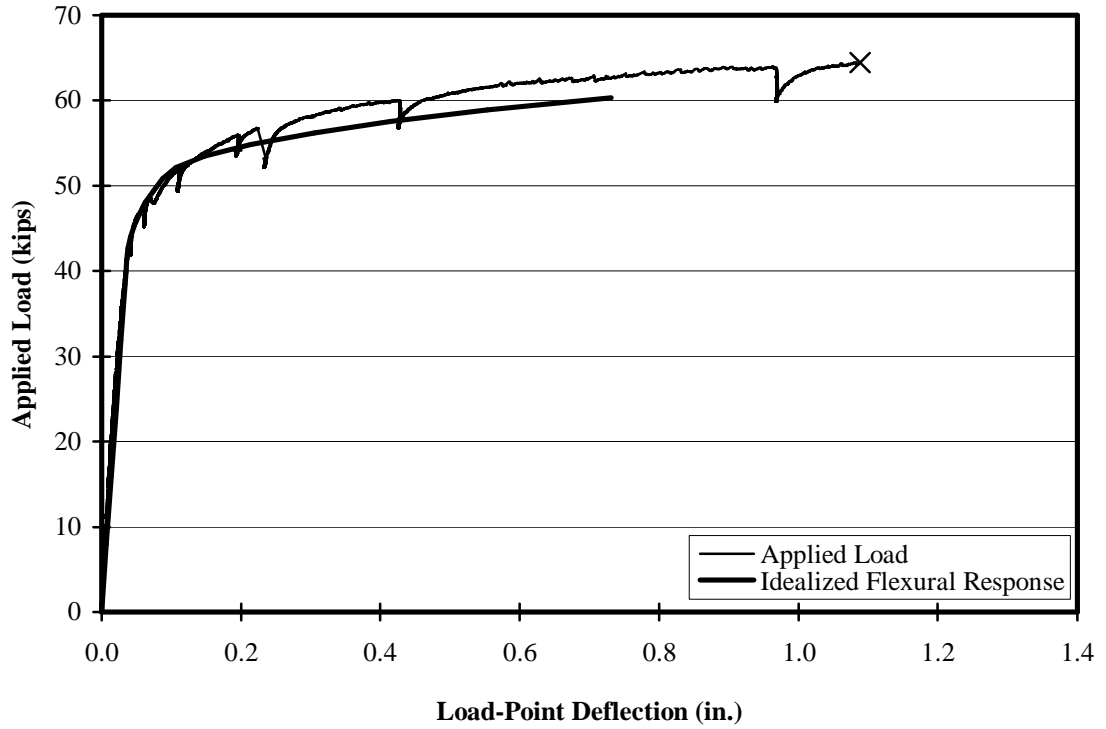


Figure 5-6. Flexural analysis result for SCC-HS-W

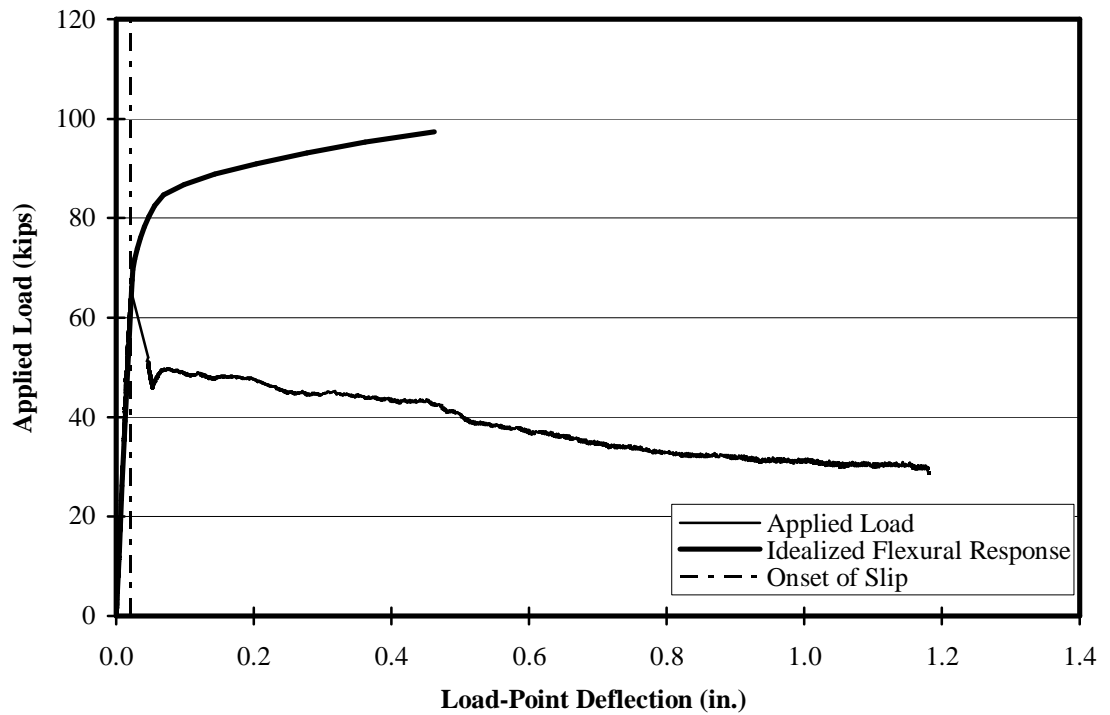


Figure 5-7. Flexural analysis result for SCC-HS-E

Table 5-1. Loads corresponding to flexural cracking and ultimate strength

Specimen	Analysis Results			Experimental Results	
	Flexural cracking load (kips)	Ultimate load (kips)	P at AASHTO M_n (kips)	Flexural (F) or shear (S) cracking load (kips)	Ultimate capacity (kips)
STD-M-E	36.2	52.6	50.2	32.1 (S)	32.1
STD-M-W	36.2	52.6	50.2	27.2 (S)	27.2
SCC-MS-E	37.8	56.2	52.5	48.1 (F)	63.1
SCC-HS-W	39.9	60.3	53.5	48.0 (F)	64.5
SCC-HS-E	65.4	97.4	86.1	66.1 (S)	66.1

In Table 5-2, analytically computed flexural cracking moments are compared with the actual moments at the locations where cracks were observed.

Table 5-2. Cracking moments corresponding to crack locations

Specimen	Analysis results	Experimental results
	Flexural cracking moment (kip-ft)	Applied moment (kip-ft) at the time and location of flexural (F) or shear (S) crack
STD-M-E	66.7	29.6 (S)
STD-M-W	66.7	21.7 (S)
SCC-MS-E	69.6	88.6 (F)
SCC-HS-W	73.5	88.4 (F)
SCC-HS-E	75.0	41.7 (S)

Specimens SCC-MS-E and SCC-HS-W, both having failed flexurally, show good agreement with flexural analysis results, while having slightly more ultimate capacity than predicted. This difference of ultimate capacity is attributed to the relative movements of support locations which caused slight changes in total span length, as well as uncertainties in material properties such as strength and modulus of elasticity and other random experimental errors.

Specimens STD-M-E, STD-M-W and SCC-HS-E each failed in a shear-tension mode of failure. Comparison with analysis results show that they reached neither flexural cracking moments nor their flexural capacities at their times of failure.

5.2. AASHTO LRFD Shear Analyses

5.2.1. Shear cracking

AASHTO LRFD (2007) provisions lack a prediction value for initial shear cracking. In this study, V_c is used as a parameter for cracking shear load. Normally, V_c is considered the concrete contribution to the shear resistance of a cracked section. If transverse reinforcement is provided, V_c is the concrete contribution to the ultimate shear capacity, not simply the shear that causes initial shear cracking. However, it is reasonable to assume that the AASHTO LRFD expression for V_c in members *without* transverse reinforcement provides a more accurate estimate of the shear corresponding to first cracking because transverse reinforcement is not engaged until after the crack forms. Therefore, all of the specimens were analyzed as if they did not have any transverse reinforcement.

Figure 5-8 shows a plot of V_c values, calculated using the AASHTO LRFD shear provisions in Section 5.8.3.3 at the critical section versus experimental ultimate loads. The critical section, a distance of d_v away from the support, is used as the section for analysis because the AASHTO LRFD specifications indicate this location is to be used for design of all sections located between the critical section and the support. The critical section was found to be the weakest among the sections between the critical section and the load point because it was within the transfer length of prestressing strands. Effective prestressing force was not fully transferred for most of the specimens at this cross section; therefore, in the calculation process, the prestressing force was adjusted for according to the bi-linear stress-distance relationship, as described by AASHTO LRFD Commentary C5.11.4.2 (2007), using experimentally determined transfer lengths and AASHTO predicted development lengths.

Three more specimens described by Levy (2007), STD-M-D, SCC-MS-D and SCC-HS-D, are also included in these results. These three additional specimens had the same cross section and were constructed with the same concrete as those described in this thesis. Specimens that did not experience shear cracks are denoted with a “+” marker as these specimens would not have experienced shear cracks until greater loads than were achieved prior to flexural failure.

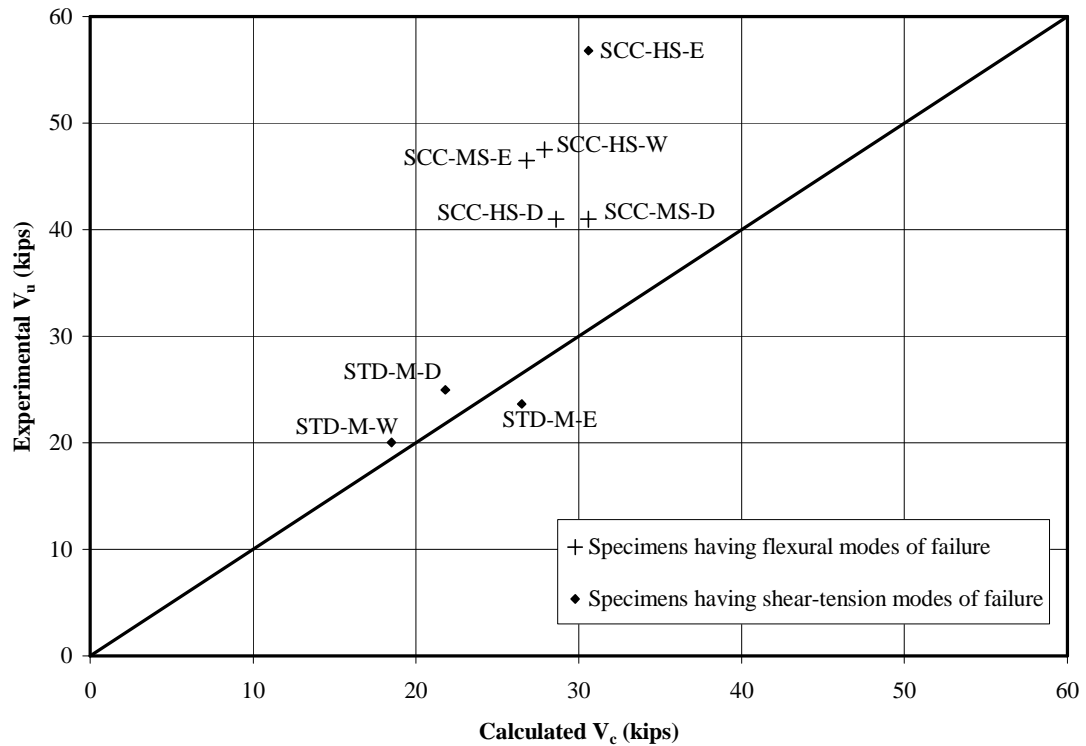


Figure 5-8. Experimental versus valuated V_c values

It can be observed that AASHTO LRFD provision for V_c is quite accurate for the moderate-strength conventionally consolidated concrete mixtures. However, for the high-strength and moderate-strength SCC, it is observed that AASHTO provisions are quite conservative. This statement is further supported by evaluating Figure 5-9, where V_c is plotted against ϵ_x for $s_{xe} \leq 15$ in. ϵ_x is the longitudinal strain in the flexural tension side of the member and s_{xe} is the crack spacing parameter. For all the tested specimens, s_{xe} was calculated to be less than the dividing value of 15 in as maximum aggregate size (a_g) was taken as $\frac{3}{4}$ in. Figure 5-9 illustrates all possible values of V_c for the allowed range of ϵ_x . It can be observed that at no ϵ_x value is V_c anywhere close to experimental results for concrete strengths other than for the 6.32-ksi conventionally consolidated concrete (STD). For those specimens that did not exhibit any diagonal cracks (SCC-MS-E, SCC-

HS-W, SCC-MS-D and SCC HS-D), ultimate loads achieved (limited by flexural failure) are substituted as a form of lower bound.

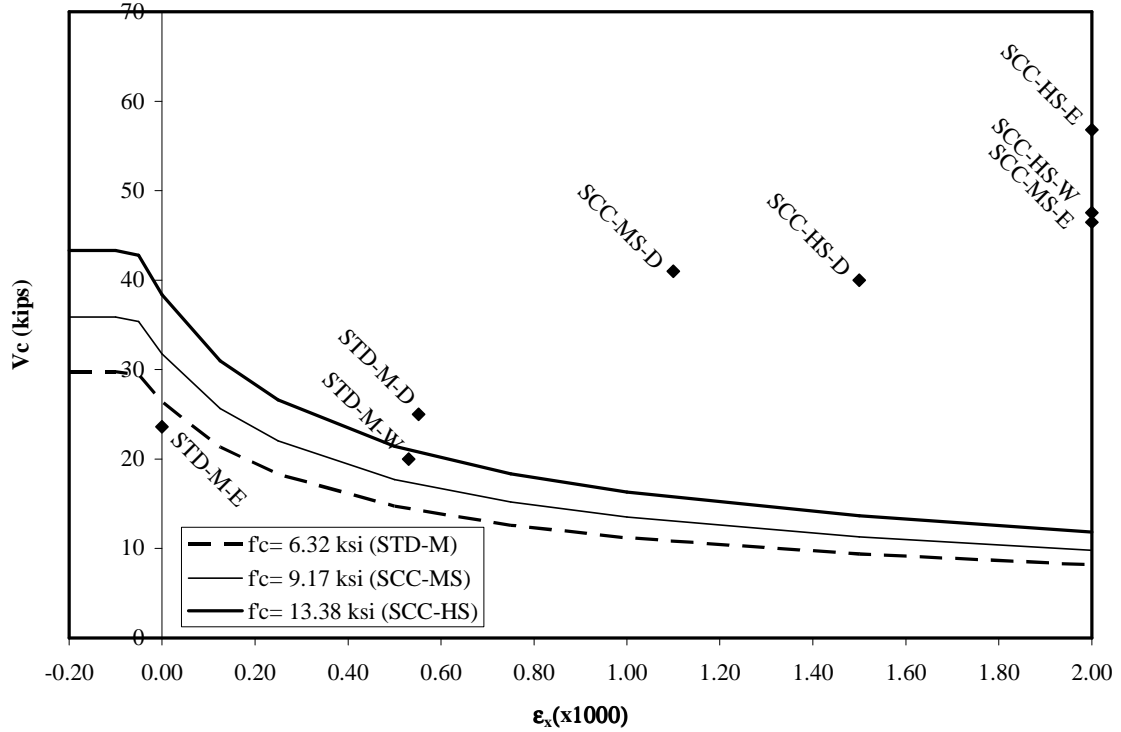


Figure 5-9. V_c as function of ϵ_x for $s_{xe} \leq 15$ in.

5.2.2. Shear capacity

AASHTO LRFD Bridge Design Specifications (2007) were used to calculate predicted nominal shear capacities (V_n) of the test specimens. Article 5.8.3.3 was followed as a guideline and the General Procedure in Article 5.8.3.4.2 was used for V_c calculations. As these are ultimate (i.e. post-cracking) capacity calculations, transverse reinforcement was taken into consideration for these V_c calculation procedures.

In the General Procedure, as described in Article 5.8.3.4.2, when the member has at least the minimum required transverse reinforcement, shear ratio (v_u/f'_c) is used a

criterion for the iteration procedure of θ and β values. Shear ratio is simply the shear stress (shear force V_u divided by $b_v d_v$) divided by concrete compressive strength. All of the tested specimens fall into the lower-bound category of $v_u/f'_c \leq 0.075$.

Table 5-3 shows calculated V_c , V_s and V_n values for the specimens as well as the maximum applied shear, V_u . These values were calculated at the critical section using the maximum applied shear during testing taken as V_u . Again, prestressing force was adjusted for using experimentally determined transfer lengths and AASHTO predicted transfer lengths.

Table 5-3. Shear capacity calculations based on applied maximum shear

Specimen	V_c (kips)	V_s (kips)	V_n (kips)	V_u (kips)	Failure mode
STD-M-E	20.4	35.8	56.2	23.6	Shear-tension
STD-M-W	15.5	27.8	43.3	20.0	Shear-tension
SCC-MS-E	15.0	19.7	34.7	46.5	Flexural/Strand slip
SCC-HS-W	18.2	19.7	37.9	47.5	Flexural/Strand slip
SCC-HS-E	18.2	19.7	37.9	55.7	Shear-tension

Table 5-4 shows calculated V_c , V_s and V_n values when V_n was taken equal to the applied maximum shear, which was taken as V_u for the computation process. This approach is closer to an actual shear design process when the capacity of a member is calculated according to the anticipated *design* load.

Table 5-4. Shear capacity calculations based on $V_n = V_u$

Specimen	V_c (kips)	V_s (kips)	V_n (kips)	$V_{max, exp}$ (kips)	Failure mode
STD-M-E	12.9	23.1	36.0	23.6	Shear-tension
STD-M-W	12.5	19.7	32.7	20.0	Shear-tension
SCC-MS-E	15.4	21.5	36.9	46.5	Flexural/Strand slip
SCC-HS-W	18.3	20.4	38.7	47.5	Flexural/Strand slip
SCC-HS-E	18.7	21.7	40.7	55.7	Shear-tension

It can be observed that AASHTO-predicted nominal shear strengths are higher than the actual shear forces resisted by the specimens with conventional concrete mixtures. The main reason is that the AASHTO V_n provisions assume a diagonal tension failure mode. In order to also address the shear-tension failure mode, AASHTO specifications include a longitudinal reinforcement check introduced in Article 5.8.3.5.

On the other hand, AASHTO-predicted nominal shear strengths are lower than the resisted shear forces in the specimens with SCC mixtures. The reason attributed to this difference is the conservatism of AASHTO LRFD specifications in case of high-strength, SCC concrete mixtures.

5.2.3. Post-cracking tension demand

Shear-tension failures observed in the experiments were typically initiated by a web-shear crack, followed by excessive prestressing strand slip and degradation of bond. AASHTO LRFD provisions provide a check for excessive demand on longitudinal reinforcement in Article 5.8.3.5. Tension demands based on shear loads and moments on

the tested specimens were compared with tension capacities calculated using AASHTO LRFD specifications per Section 5.11. Experimental values of transfer lengths were used in these calculations, instead of AASHTO-predicted transfer lengths, in order to more realistically represent tested specimens.

Three specimens with shear-tension failure modes were analyzed for tension demand and capacity of prestressing tendons at the critical section (as defined by AASHTO) at the experimental cracking load (as reported in Chapter 4). Levy (2007) specimen STD-M-D was also added because of the similarity in test geometry. Table 5-5 shows the results of these calculations.

Table 5-5. Tension demands compared to tension capacities

Specimen	Tension Demand (ksi)	Tension Capacity (ksi)
STD-M-E	156	128
STD-M-W	117	77
STD-M-D	144	106
SCC-HS-E	357	147

Tension demand exceeding the tension capacity is essentially the cause of excessive strand slips, as well as the sudden drop in capacity of the member after a single diagonal crack.

The remaining two specimens, SCC-MS-E and SCC-HS-W, were not analyzed for tension capacity of tendons because the AASHTO LRFD approach was derived based on equilibrium conditions *after* inclined cracking at the relevant cross section. These specimens did not experience shear-influenced cracking.

Shear capacities of the three specimens STD-M-E, STD-M-W and SCC-HS-E were calculated assuming that the tension demand on the prestressing strands at the AASHTO critical section controls the maximum allowable load. Figure 5-10 thru Figure 5-12 show the applied loads that cause the strands to equal their capacity at the critical section, calculated per AASHTO LRFD specifications Article 5.8.3.5.

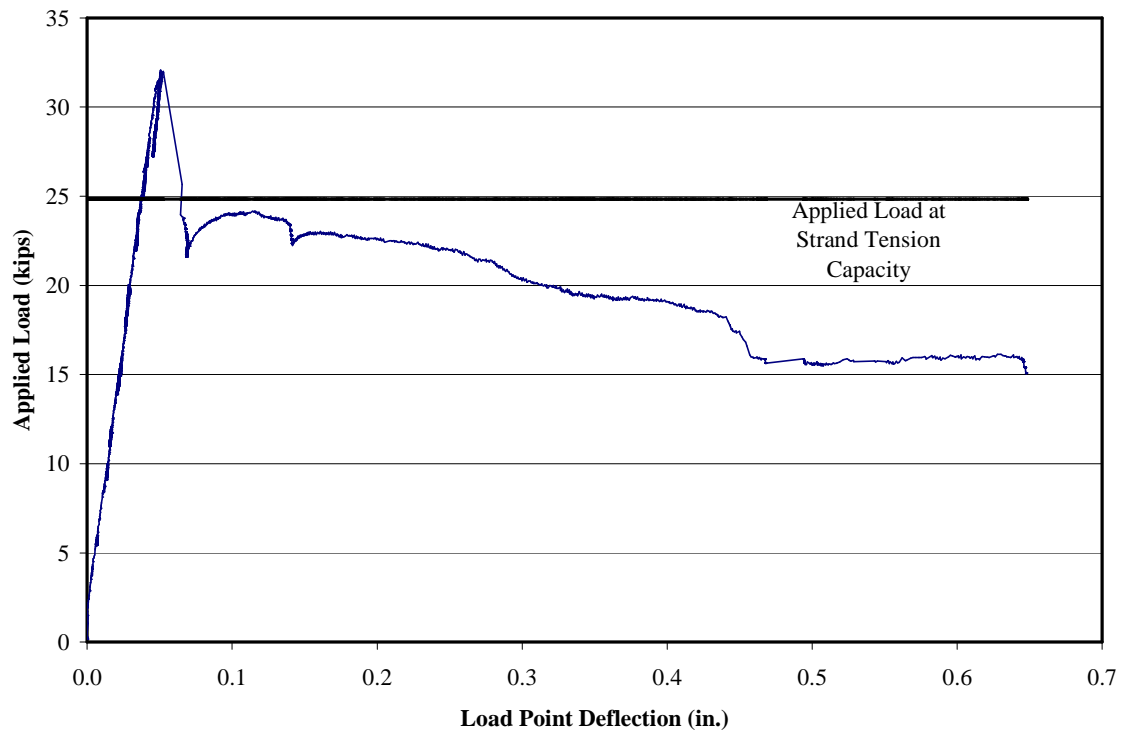


Figure 5-10. Applied load at strand tension capacity for specimen STD-M-E

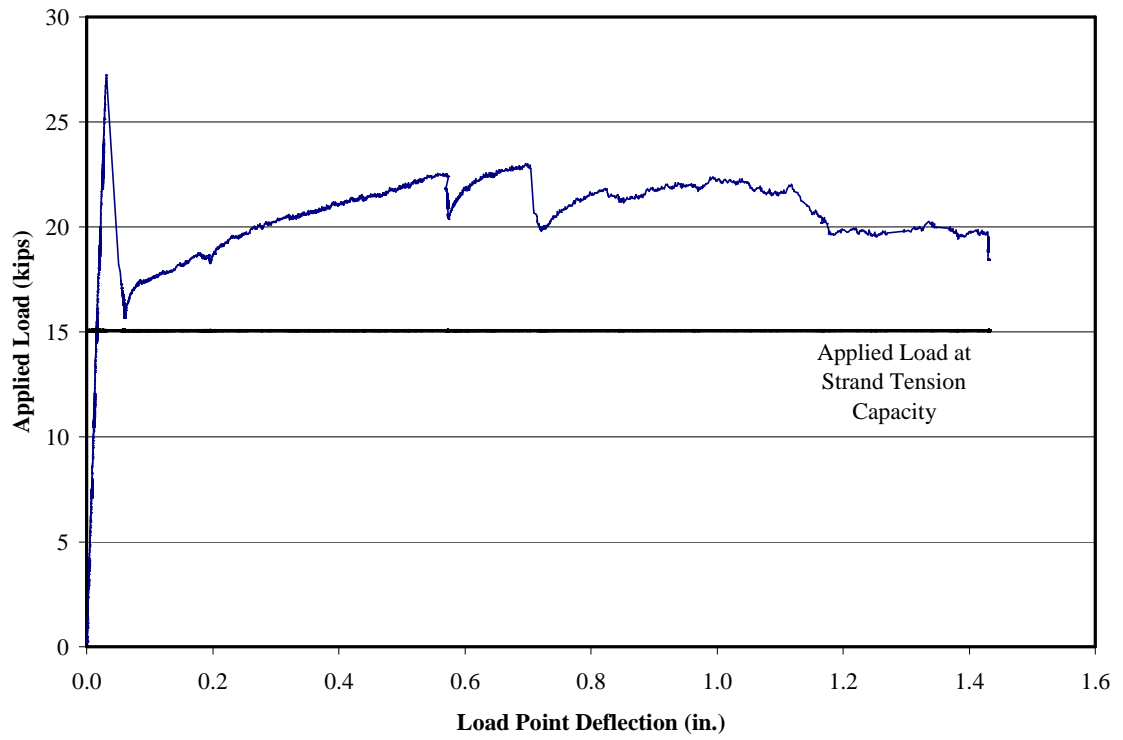


Figure 5-11. Applied load at strand tension capacity for specimen STD-M-W

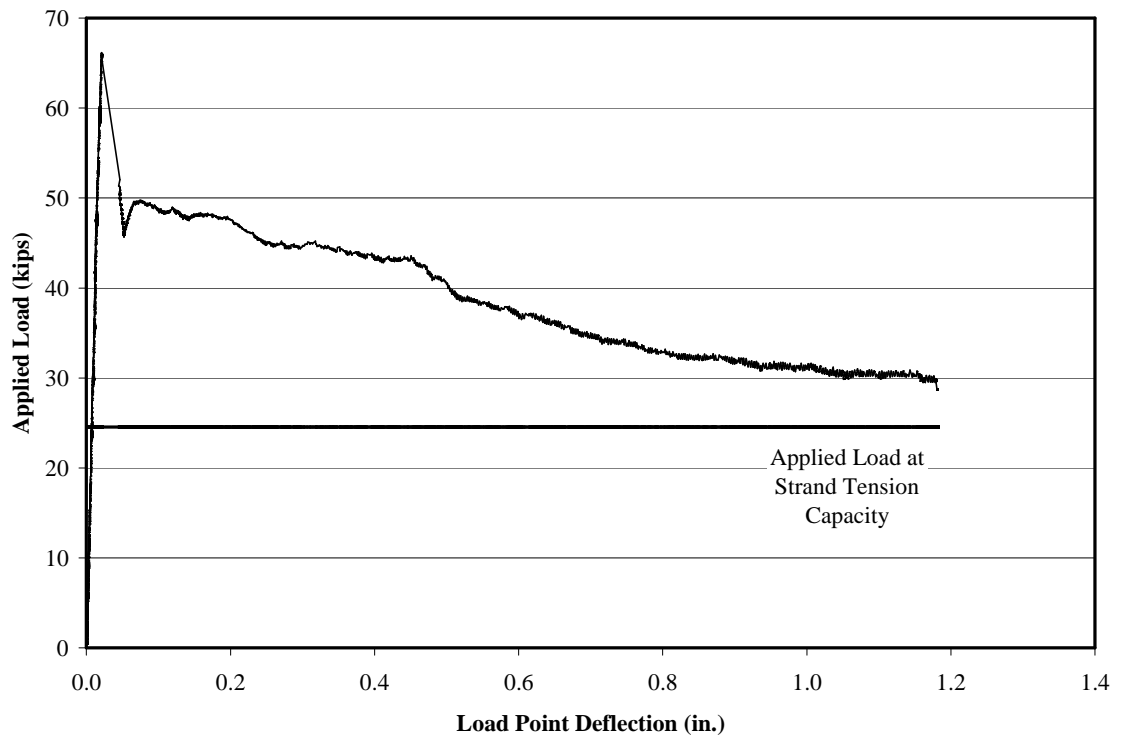


Figure 5-12. Applied load at strand tension capacity for specimen SCC-HS-E

Figure 5-14 demonstrates an increasing trend of the load after diagonal cracking as opposed to a decreasing trend as can be seen on other specimens with diagonal cracks. This behavior is attributed to the centered position of the stirrup seizing the diagonal crack and engaging more effectively in shear load resistance.

5.3. Transverse Reinforcement

5.3.1. Effect of transverse reinforcement on post-cracking tension demand

Because the stirrups did not intercept the diagonal cracks in some of the specimens, the previous analysis for post-cracking tension demand on prestressing strands was repeated for the case when the specimens were assumed not to have any transverse reinforcement.

Shear capacities of the three specimens STD-M-E, STD-M-W and SCC-HS-E were calculated assuming that the tension demand on the prestressing strands at the AASHTO critical section controls the maximum allowable load. Figure 5-13 thru Figure 5-15 show the applied loads that cause the strands to equal their capacity at the critical section, calculated per AASHTO LRFD specifications Article 5.8.3.5 for both with and without transverse reinforcement.

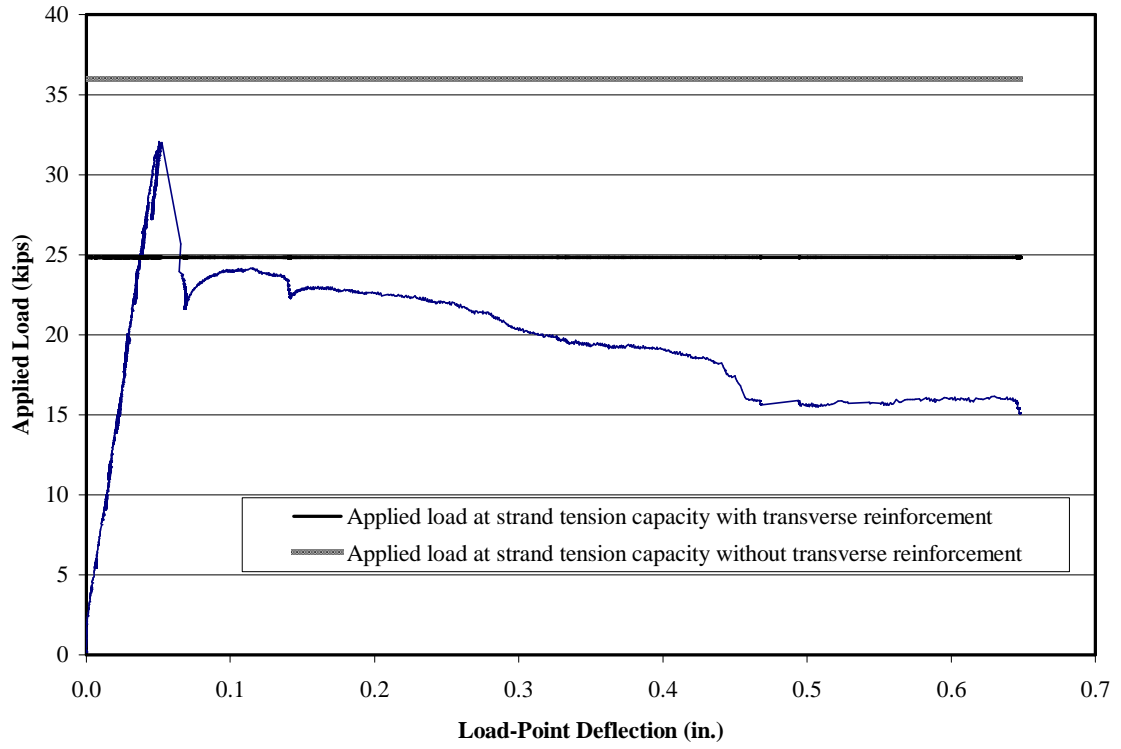


Figure 5-13. Applied load at strand tension capacity for specimen STD-M-E with and without transverse reinforcement

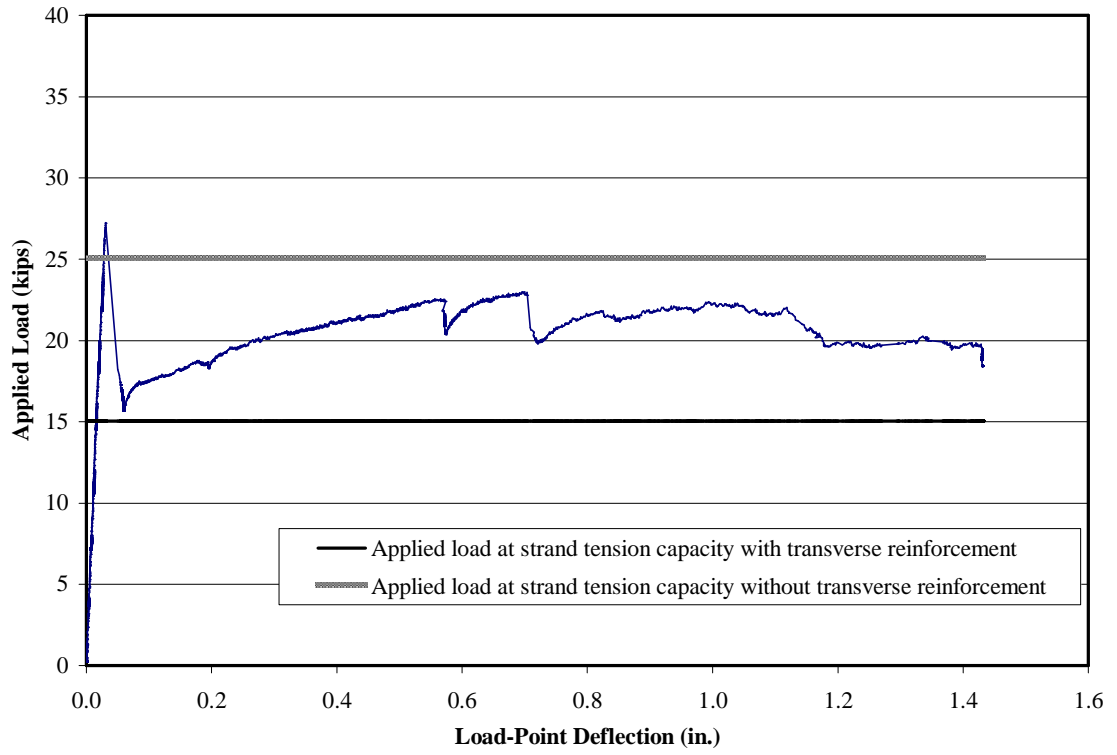


Figure 5-14. Applied load at strand tension capacity for specimen STD-M-W with and without transverse reinforcement

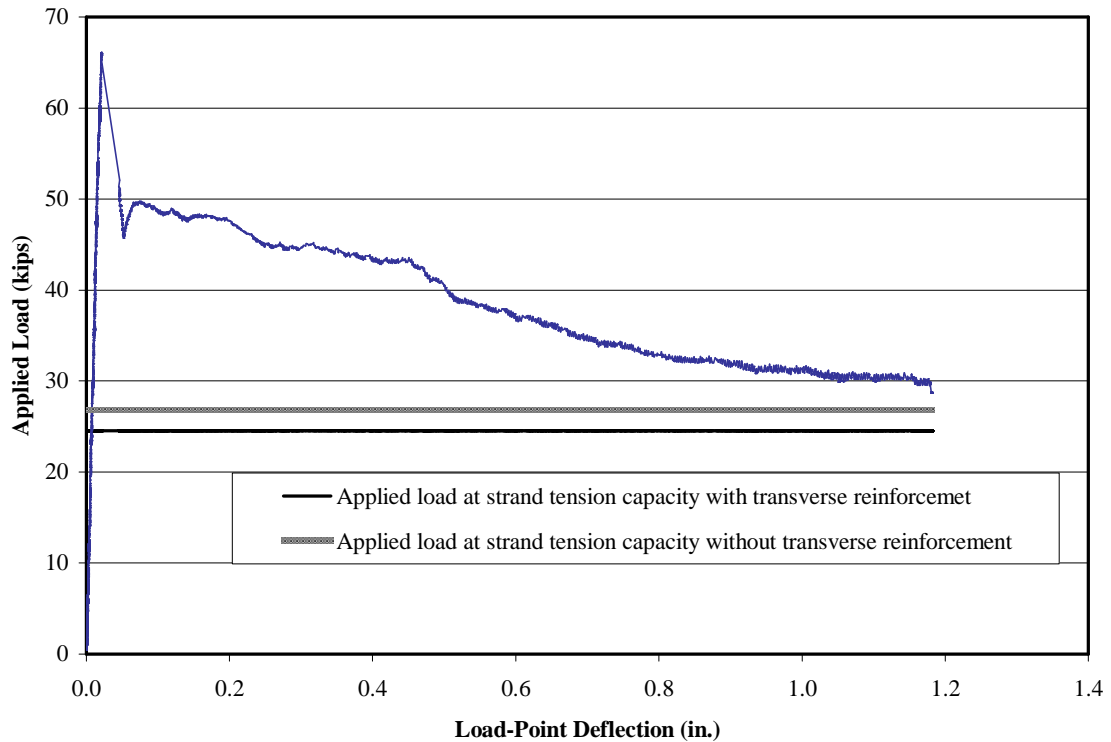


Figure 5-15. Applied load at strand tension capacity for specimen SCC-HS-E with and without transverse reinforcement

It can be observed from the graphs that the AASHTO LRFD specifications yield lower tension demands for the same specimens without transverse reinforcements. Analysis results show that AASHTO LRFD shear provisions are not conservative for members having none or less than minimum transverse reinforcement. Therefore, it is more safe to use transverse reinforcement if AASHTO LRFD specifications are to be used for design.

5.3.2. Transverse reinforcement spacing

Post-cracking reserve strengths, which refer to the capacity of the member after diagonal cracking, of the members STD-M-E, STD-M-W and SCC-HS-E are shown in Table 5-6

together with cracking loads and reserve strength as a percentage of cracking strength. Reserve strength refers to the capacity of the member after diagonal cracking.

Table 5-6. Cracking loads and reserve strengths of specimens

Specimen	Cracking Load (kips)	Reserve Load (kips)	Reserve Load as Percentage of Cracking Load
STD-M-E	32.1	24.1	75%
STD-M-W	27.2	23.0	84%
STD-HS-E	66.1	49.7	75%

It can be observed that specimen STD-M-W has significantly higher reserve strength when compared to the other specimens with diagonal cracks, as well as an increasing load resistance trend after the initial shear crack as can be seen in Figure 4-7. The difference is due to the position of the stirrups relative to the diagonal crack. Both STD-M-E and SCC-HS-E exhibited diagonal cracks that passed *between* two stirrup locations as can be seen in Figure 5-16 and Figure 5-17. On the other hand, STD-M-W had a stirrup in the middle of the diagonal crack as can be seen in Figure 5-18. This position of the diagonal crack enables the stirrup to seize the crack before it is too wide and to increase the reserve capacity of the specimen.

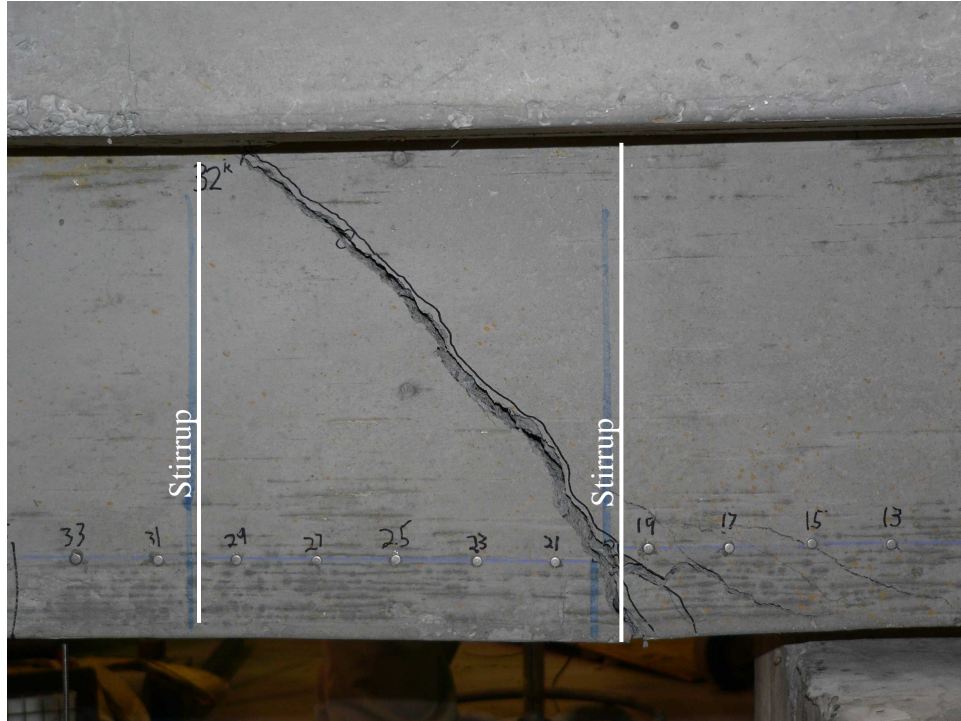


Figure 5-16. Diagonal crack location of specimen STD-M-E

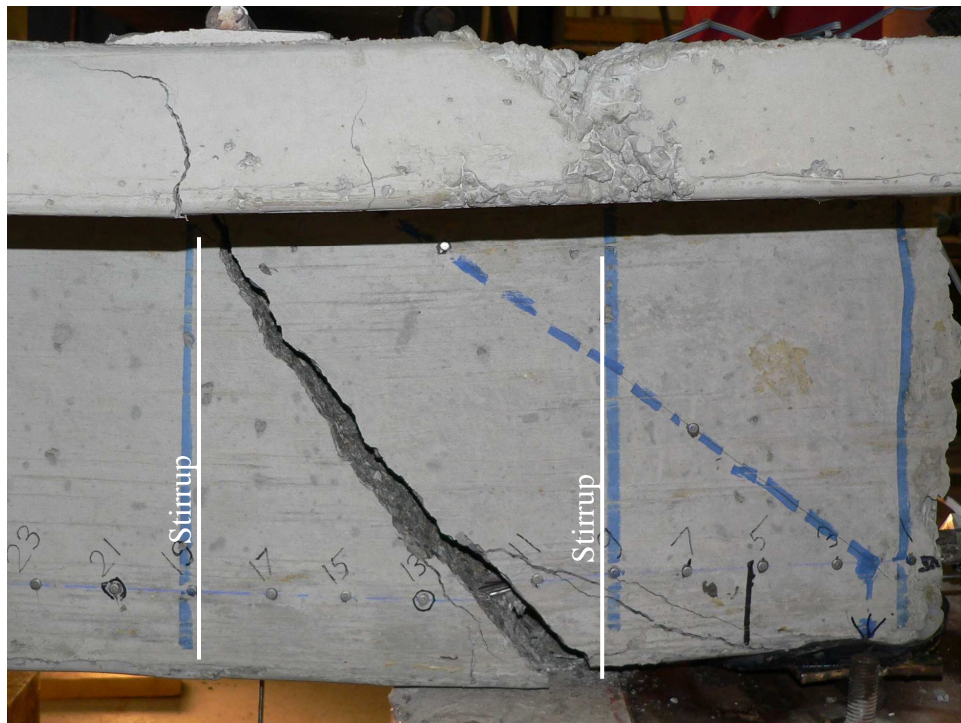


Figure 5-17. Diagonal crack location of specimen SCC-HS-E



Figure 5-18. Diagonal crack location of specimen SCC-M-W

AASHTO LRFD specifications have provisions related to transverse reinforcement spacing in Article 5.8.3.3. Required stirrup spacing for three specimens, STD-M-E, STD-M-W and SCC-HS-E were calculated, and it was found that the maximum stirrup spacing calculated per Article 5.8.2.7 controls the design. s_{max} ($0.8d_v$) is found to be 9.36 in.—a little less than the supplied spacing of 10 in.

From the behavior of specimens STD-M-E and SCC-HS-E, it is clear that the AASHTO LRFD maximum transverse reinforcement spacing requirement of $0.8d_v$ is not always effective in providing each diagonal crack with at least one intercepting stirrup. Based on the AASHTO LRFD specifications, the following relationship is derived providing a conservative requirement for s_{max} (maximum stirrup spacing) using s_{xe} (spacing parameter calculated per Article 5.8.3.4.2) and d_v (effective shear depth):

$$s_{\max} = \frac{1.6}{\sqrt{s_{xe}}} d_v$$

where, both s_{\max} and s_{xe} are in inches. This equation is implicitly making use of conservative diagonal compressive stress inclinations. Figure 5-19 show variation of s_{\max} with respect to d_v at several a_g (maximum aggregate size) values.

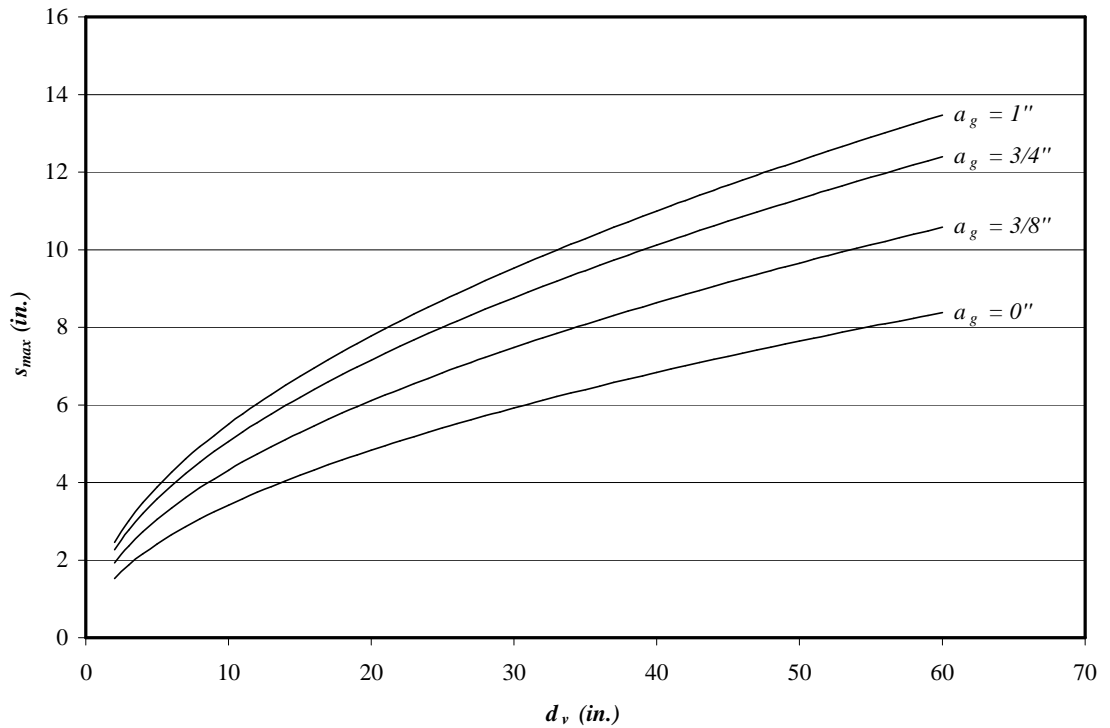


Figure 5-19. s_{\max} (maximum stirrup spacing) versus of d_v (effective shear depth)

Chapter 6. Conclusion and Recommendations

6.1. Summary

Prestressed self-consolidating concrete (SCC) is not fully understood in terms of shear and bond behavior. Therefore, more research was required in this field before full employment of SCC in prestressed concrete systems.

In order to investigate the shear and bond performance of end regions of prestressed SCC beams, five prestressed concrete beams were tested in this study with single-point loading positioned to create unequal shear spans. There were both conventionally consolidated concrete and SCC mixtures. Both shear-tension and flexural failure modes were observed.

Experimental results were compared to computed flexural analysis results and AASHTO LRFD shear design provisions. Because current AASHTO LRFD design provisions for maximum stirrup spacing proved inadequate for some of the test specimens, a simple relationship for determining maximum stirrup spacing is proposed.

6.2. Conclusions

The following conclusions can be drawn as a result of this study:

1. SCC performed better under shear than a similar-strength, conventionally consolidated concrete mixture in prestressed concrete beams.

2. SCC prestressed end regions performed at least as well under external load as the performance predicted by AASHTO LRFD design provisions for flexure, shear, and development of tension reinforcement.
3. Concrete contribution to shear resistance (V_c) when the members are assumed not to have any transverse reinforcement can be used to estimate shear cracking strengths of members.
4. AASHTO LRFD provisions can be used to accurately estimate shear cracking strength of prestressed concrete beams having conventionally consolidated concrete mixtures.
5. AASHTO LRFD provisions are overly conservative in estimating shear cracking strength of prestressed concrete beams having conventionally consolidated concrete mixtures.
6. AASHTO LRFD specifications are not conservative in estimating tension demands on longitudinal reinforcement when no transverse reinforcement is used.
7. Use of transverse reinforcement is an effective means of increasing post-cracking capacities of members that experience shear-tension failures.
8. Maximum transverse reinforcement spacing provided by AASHTO LRFD specifications is not conservative because diagonal cracks can occur that are not crossed by at least one stirrup.

6.3. Recommendations

The following recommendations are suggested:

1. SCC mixtures with a wider variety of strengths should be tested for shear performance and compared to conventional concrete mixtures.
2. Further SCC research regarding shear behavior is necessary.
3. High-strength concrete should be more adequately addressed by AASHTO

LRFD specifications enabling engineers to take advantage of more efficient mixture designs.

4. The general procedure in AASHTO LRFD shear provisions should be extended to cover a wider range of concrete strengths.

5. The following equation is recommended for the determination of maximum stirrup spacing:

$$s_{\max} = \frac{1.6}{\sqrt{s_{xe}}} d_v$$

References

- AASHTO. 2007. *AASHTO LRFD Bridge Design Specifications*. 4th Edition. Washington D.C. American Association of State Highway Transportation Officials.
- ACI Committee 318. 2005. *Building Code Requirements for Structural Concrete and Commentary*. Farmington Hills: American Concrete Institute.
- Angelakos, D., E. C. Bentz, and M. P. Collins. 2001. Effect of Concrete Strength and Minimum Stirrups on Shear Strength of Large Members. *ACI Structural Journal* 98: 290-300.
- ASCE-ACI Joint Task Committee 426. 1973. The Shear Strength of Reinforced Concrete Members. *Journal of the Structural Division: ASCE* 99: 1091-1187.
- Beer, F. P., E. R. Johnston, Jr. 1992. *Mechanics of Materials*. 2nd Edition in SI Units. England. McGraw-Hill.
- Bentz, E. C., F. J. Vecchio, and V. Collins. 2006. Simplified Modified Compression Field Theory for Calculating Shear Strength of Reinforced Concrete Elements. *ACI Structural Journal* 103: 614-624.
- Bentz, E. C., and V. Collins. 2006. Development of Canadian Standards Association (CSA) A23.3 Shear Provisions for Reinforced Concrete. *Canadian Journal of Civil Engineering* 33: 521-534.
- Bresler, B., and J. G. MacGregor. 1967. Review of Concrete Beams Failing in Shear. *Journal of the Structural Division: ASCE* 93: 343-372.
- Collins, M. P. 1978. Towards a Rational Theory for RC Members in Shear. *Journal of The Structural Division: ASCE* 104: 649-666.
- Collins, M. P., and D. Mitchell. 1997. *Prestressed Concrete Structures*. Toronto. Response Publications.
- Cook, W. D., and D. Mitchell. 1988. Studies of Disturbed Regions Near Discontinuities in Reinforced Concrete Members. *ACI Structural Journal* 85: 206-216.
- Fenwick, R. C., T. Paulay. 1968. Mechanism of Shear Resistance of Concrete Beams. *Journal of the Structural Division: ASCE* 94: 2325-2350.

Ferguson, P. M., J. E. Breen, and J. O. Jirsa. 1988. *Reinforced Concrete Fundamentals*. 5th Edition. New York. Wiley.

Hawkins, N. M., D. A. Kuchma, R. F. Mast, M. L. Marsh, and K. Reineck. 2005. *NCHRP Report 549: Simplified Shear Design of Structural Concrete Members*. Washington. D.C. Transportation Research Board.

Lorensten, M. 1965. Theory for the Combined Action of Bending Moment and Shear in Reinforced and Prestressed Concrete Beams. *Journal of the American Concrete Institute* 62: 403-420.

Levy, K. R. 2007. Bond Behavior of Prestressed Reinforcement in Beams Constructed with Self-Consolidating Concrete. M.S. Thesis. Auburn University

Nawy, E. G. 2006. *Prestressed Concrete: A Fundamental Approach*. 5th Edition. New Jersey. Pearson Prentice Hall.

MacGregor, J. G., and J. M. Hanson. 1969. Proposed Changes in Shear Provisions for Reinforced and Prestressed Concrete Beams. *ACI Journal* 66: 276-288.

MacGregor, J. G., M. A. Sozen, and C. P. Siess. 1965. Strength of Prestressed Concrete Beams with Web Reinforcement. *Journal of the American Concrete Institute: Proceedings* 62: 1503-1519.

Moe, J. 1962. Discussion of: Shear and Diagonal Tension. *ACI Journal: Proceedings* 59: 1334-1339.

Naaman, A. E. 2004. *Prestressed Concrete Analysis and Design: Fundamentals*. 2nd Edition. Ann Arbor. Techno Press 3000.

Ozcebe, G., U. Ersoy, and T. Tankut. 1999 Evaluation of Minimum Shear Reinforcement Requirements for Higher Strength Concrete. *ACI Structural Journal* 96: 361-369.

Rahal, K. N., and K. S. Al-Shaleh. 2004. Minimum Transverse Reinforcement in 5 MPa Concrete Beams. *ACI Structural Journal* 101: 872-878.

Roberts, J. 2005. Evaluation of Self-Consolidating Concrete for Use in Prestressed Girder Applications. M.S. Thesis. Auburn University.

Sherwood, E.G., E. C. Bentz, and M. P. Collins. 2007. Effect of Aggregate Size on Beam-Shear Strength of Thick Slabs. *ACI Structural Journal* 104: 180-190.

Sozen, M. A., and N. M. Hawkins. 1962. Discussion of: Shear and Diagonal Tension. *ACI Journal, Proceedings* 59: 1341-1347.

Swords, S. 2005. Transfer Length in Prestressed Self-Consolidating Concrete. M.S. Thesis., Auburn University.

Vecchio, F. J., and M. P. Collins. 1986. The Modified Compression-Field Theory for Reinforced Concrete Elements Subjected to Shear. *ACI Journal* 83: 219-231.

Appendix A. Notation

a	shear span
a_g	maximum aggregate size
A_{ps}	area of prestressing steel
A_s	area of mild tension reinforcement
A_v	area of transverse reinforcement within distance s
β	factor relating effect of longitudinal strain to the shear capacity of concrete
b_v, b_w	width of web
d	depth of tension reinforcement
d_v	effective shear depth
E_c	modulus of elasticity of concrete
E_p	modulus of elasticity of prestressing reinforcement
E_s	modulus of elasticity of mild steel reinforcement
ε_1	strain in direction of principal tension
ε_2	strain in direction of principal compression
ε_p	strain in prestressing reinforcement

ϵ_x	longitudinal strain on the flexural tension side of the member
f_1	stress in direction of principal tension
f_2	stress in direction of principal compression
f'_c	specified compressive strength of concrete
$f_{c,28}$	specified compressive strength of concrete at 28 days
f_{cr}	cracking stress of concrete
f_{du}	limiting value of the average principal compressive stress in concrete
f_{ly}	yield strength of longitudinal mild reinforcement
f_p	stress in prestressing reinforcement
f_{pe}	effective stress in prestressed reinforcement after losses
f_{pj}	stress in prestressing steel after jacking
f_{ps}	stress in prestressed reinforcement at the estimated nominal strength estimated by AASHTO prior to flexural testing
f_{py}	yield strength of prestressing reinforcement
f_r	modulus of rupture
f_t	splitting tensile strength
f_{ty}	yield strength of transverse reinforcement
f_y	yield stress of mild steel reinforcement
I	moment of inertia

jd	effective depth for shear
$l_{t,exp.}$	experimentally determined transfer length
$l_{d,AASHTO}$	development length estimated by AASHTO with calculated properties
M_n	predicted nominal moment capacity according to AASHTO LRFD specifications
M_n	factored moment at section
N	axial force
Q	first moment of area about the neutral axis
ρ_l	longitudinal mild reinforcement ratio
ρ_p	prestressing reinforcement ratio
ρ_t	transverse reinforcement ratio
s	transverse reinforcement spacing
s_{max}	maximum permitted transverse reinforcement spacing
s_x, s_{xe}	crack spacing parameters
σ	axial stress
t	thickness
τ	shear stress
τ_{ave}	width-averaged shear stress
θ	angle of inclination of diagonal compressive stresses

V	shear stress
V_c	nominal shear resistance provided by tensile stresses in concrete
V_n	nominal shear resistance of the section considered
V_p	component in the direction of applied shear of the prestressing force
V_s	shear resistance provided by shear reinforcement
v_u	average factored shear stress on the concrete
V_u	factored shear force at section